Basin Research (2009) doi: 10.1111/j.1365-2117.2009.00431.x

Insights in the exhumation history of the NW Zagros from bedrock and detrital apatite fission-track analysis: evidence for a long-lived orogeny

Stéphane Homke,* Jaume Vergés,* Peter van der Beek,† Manel Fernàndez,* Eduard Saura,* Luis Barbero,‡ Balazs Badics§ and Erika Labrin†

*Group of Dynamics of the Lithosphere (GDL), Institute of Earth Sciences 'Jaume Almera', CSIC, Barcelona, Spain
†Laboratoire de Géodynamique des Chaînes Alpines, UMR CNRS 5025, Université Joseph Fourier, 38041 Grenoble, France
‡Departamento de Ciencias de la Tierra, Universidad de Cádiz, Cádiz, Spain
§Statoilhydro INT Global Exploration, Global Screening, 4034 Stavanger, Norway

ABSTRACT

We present the first fission-track (FT) thermochronology results for the NW Zagros Belt (SW Iran) in order to identify denudation episodes that occurred during the protracted Zagros orogeny. Samples were collected from the two main detrital successions of the NW Zagros foreland basin: the Palaeocene–early Eocene Amiran–Kashkan succession and the Miocene Agha Jari and Bakhtyari Formations. *In situ* bedrock samples were furthermore collected in the Sanandaj-Sirjan Zone. Only apatite fission-track (AFT) data have been successfully obtained, including 26 ages and 11 track-length distributions. Five families of AFT ages have been documented from analyses of *in situ* bedrock and detrital samples: pre-middle Jurassic at ~171 and ~225 Ma, early–late Cretaceous at ~91 Ma, Maastrichtian at ~66 Ma, middle–late Eocene at ~38 Ma and Oligocene–early Miocene at ~22 Ma. The most widespread middle–late Eocene cooling phase, around ~38 Ma, is documented by a predominant grain-age population in Agha Jari sediments and by cooling ages of a granitic boulder sample. AFT ages document at least three cooling/denudation periods linked to major geodynamic events related to the Zagros orogeny, during the late Cretaceous oceanic obduction event, during the middle and late Eocene and during the early Miocene. Both late Cretaceous and early Miocene orogenic processes produced bending of the Arabian plate and concomitant foreland deposition. Between the two major flexural foreland episodes, the middle–late Eocene phase mostly produced a long-lasting slow- or nondepositional episode in the inner part of the foreland basin, whereas deposition and tectonics migrated to the NE along the Sanandaj-Sirjan domain and its Gaveh Rud fore-arc basin. As evidenced in this study, the Zagros orogeny was long-lived and multi-episodic, implying that the timing of accretion of the different tectonic domains that form the Zagros Mountains requires cautious interpretation.

INTRODUCTION

The formation of the Zagros Fold Belt is the result of the convergence between Arabia and Eurasia, which culminated with the final closure of the Neo-Tethys oceanic domain producing the continental collision of these two plates (Fig. 1). Orogenic processes started with the tectonic emplacement of ophiolitic slices over the NE Arabian passive margin, from SE Turkey to Oman, at the end of Cretaceous times (e.g. Stöcklin, 1968; Ricou *et al.*, 1977; Berberian & King, 1981; Braud, 1987; Stoneley, 1990; Ravaut *et al.*, 1997; Babaei *et al.*, 2005).

Correspondence: Stéphane Homke, StatoilHydro Research Centre, Bergen, PO Box 7190, N-5020 Bergen, Norway. E-mail: sthom@statoilhydro.com.

The complete late Cretaceous and Tertiary history of this protracted collision is still debated, because multiple collisions of small continental blocks and island arcs against the NE Arabian margin are recorded. Based on ages of calc-alkaline magmatism, Berberian *et al.* (1982) proposed that the Arabia–Eurasia collision occurred in late Paleogene or early Neogene times. Hooper *et al.* (1994) suggested that the Neo-Tethys suture was diachronous, progressing towards the SE with final ocean consumption in late Oligocene times. Using plate tectonic reconstructions, McQuarrie *et al.* (2003) calculated a minimum age for final Arabia–Eurasia closure at 10 Ma (late Miocene). On the basis of seawater circulation and continental faunal exchanges, it has been argued that continental collision took place in the late Burdigalian times,

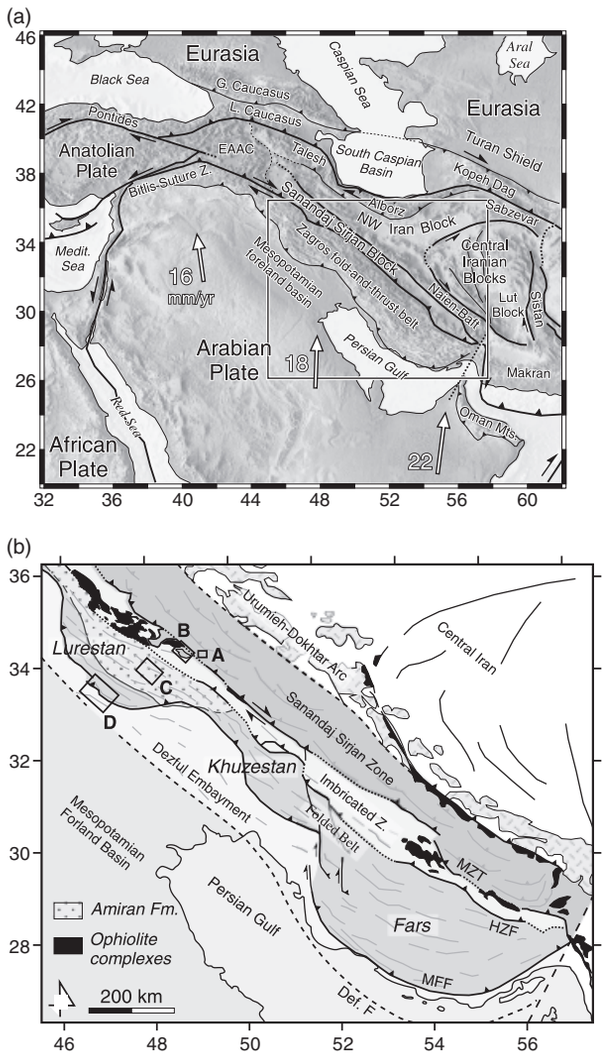

Fig. 1. (a) Plate tectonic context of the Arabian–Eurasian collision zone. Relative plate velocities of Arabia with respect to Eurasia, given in mm year^{-1}, are from Sella *et al.* (2002). Location of Map B is indicated. EAAC, East Anatolian Accretionary Complex. (b) Structural map of the Zagros orogenic domain. Ophiolite–radiolarite complexes are mapped in black. The boundary of the Amiran flexural basin is indicated. Maps represented in Fig. 4 are located by boxes A–D. MZT, main Zagros thrust; HZF, high Zagros fault; MFF, Mountain front fault; Def. F, deformation front.

synchronous to the formation of an important emerged landbridge (i.e. the 'Gomphotherium Landbridge') between Africa–Arabia and Eurasia (Rögl, 1998; Harzhauser *et al.*, 2007). At a more regional scale, the structural observations of Hempton (1985, 1987) and Robertson (2006) have shown that continental collision in SE Turkey, along the so-called Bitlis suture zone, initiated during middle–late Eocene and lasted until middle–late Miocene (Fig. 1a). On the basis of structural observations and biostratigraphic ages of sediments located to the NE of our study area, Agard *et al.* (2005) proposed that final continental collision in the NW Zagros was initiated before latest Oligocene time, in agreement with results from Horton *et al.* (2008). This age is compatible with the early Miocene age of the most proximal exposures of the syn-orogenic Bakhtyari Formation close to the Main Zagros Thrust, recently dated by Fakhari *et al.* (2008). In the Fars, more to the SW, the onset of foreland development and the initiation of tectonic inversion occurred slightly later at 20 Ma (Mouthereau *et al.*, 2007).

The difficulties in unravelling this long history led us to initiate precise dating of detrital foreland sequences in order to constrain the foreland basin history (Homke *et al.*, 2009), together with a thermochronology study that is presented in this paper. The aim of this study is to constrain the cooling/denudation events related to the protracted tectonic evolution that shaped the Zagros Mountains, using a combination of detrital and *in situ* apatite fission-track (AFT) thermochronology. Detrital apatites have been sampled from two well-dated sedimentary sequences located in the NW Zagros Fold Belt (Pusht-e Kuh Arc in Lurestan Province): the Paleocene Amiran Formation in the Amiran and Sultan anticlines and the middle and late Miocene Agha Jari Formation in the Afrineh and Changuleh growth synclines. In addition, granite boulders from folded conglomerates attributed to the Neogene Bakhtyari Formation in the Imbricated Zone have been sampled. *In situ* bedrock samples have been collected in metamorphic rocks of the Sanandaj-Sirjan Zone (Fig. 1b). The resulting inferred cooling events are integrated with published regional reconstructions in order to better constrain the tectonic evolution of the Zagros Belt through time.

GEOLOGICAL OVERVIEW OF THE ZAGROS BELT

The NW–SE trending Zagros Mountain Belt is constituted by five different parallel structural domains, from SW to NE: (1) the Mesopotamian-Persian Gulf foreland basin, (2) the Folded Belt, (3) the Imbricated Zone (also called High Zagros or Crush Zone), (4) the metamorphic and magmatic Sanandaj-Sirjan Zone and (5) the Urumieh-Doktar magmatic arc (Fig. 1). In this section we present the geological setting of these structural domains, with special emphasis on the NW Zagros Belt where we focussed our work (Fig. 1b).

The Folded Belt and the Mesopotamian foreland basin

The Mesopotamian Plain and its SE continuation along the Persian Gulf form the foreland basin in front of the Folded Belt (Fig. 1). The Folded Belt is characterized by spectacularly outcropping anticlines involving the complete 10–12-km-thick Arabian margin succession (e.g. Falcon, 1974; Colman-Sadd, 1978). The Mountain Front Fault (or Mountain Front Flexure, MFF) bounds the Folded Belt to the SW (Falcon, 1961; Emami *et al.*, in press). This structural and topographic front has an irregular geome-

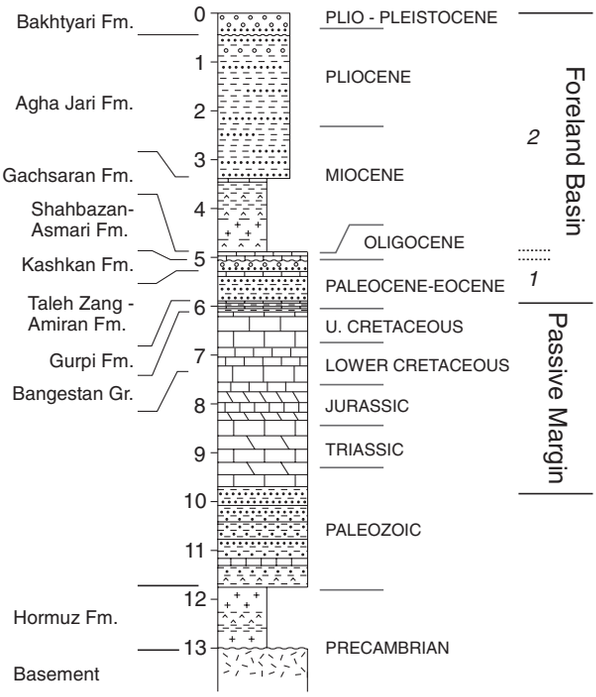

Fig. 2. Schematic stratigraphic column of the Zagros sedimentary cover in central Lurestan Province. Thickness in kilometres. Amiran–Kashkan and Gachsaran–Agha Jari–Backtyari detrital foreland successions are marked 1 and 2.

try forming two salients, the Fars Arc (Fars Province) and the Pusht-e Kuh Arc (Lurestan Province), separated by the Dezful Embayment (Khuzestan Province). The Folded Belt is limited to the NE by the so-called High Zagros Fault (Berberian, 1995) (Fig. 1b). The folding along the frontal regions of the Pusht-e Kuh Arc, characterized by multiple detachments (Vergés *et al.*, in press), started around 7.6 ± 0.5 Ma and lasted until the Pliocene–Pleistocene boundary at about 2.5 Ma (Homke *et al.*, 2004) although folding occurred earlier in the more internal domains of the belt (Emami, 2008).

In Lurestan Province, the exposed Mesozoic–Cenozoic stratigraphy includes about 4–5 km of pre-orogenic strata and about 4–5 km of synorogenic deposits (Fig. 2). The synorogenic strata include two detrital successions related to early development of the foreland basin and to Miocene–Pliocene folding, respectively (James & Wynd, 1965; Homke *et al.*, 2004). The turbiditic Amiran Formation, the carbonaceous Taleh Zang Formation and the conglomeratic Kashkan Formation constitute a shallowing upwards sequence that filled an early foreland basin developed as a consequence of the emplacement of ophiolitic and radiolaritic thrust sheets over the Arabian platform (e.g. Alavi, 1994; Homke *et al.*, 2009). Deposition of these sediments was synchronous with folding affecting this early Zagros foreland basin (Hessami *et al.*, 2001; Fakhari & Soleimany, 2003; Sherkati & Letouzey, 2004; Blanc *et al.*, 2008; Homke *et al.*, 2009).

The Amiran and Taleh Zang Formations have been accurately dated by nannoplankton biostratigraphy (very accurate for the lower part of the succession) and benthic foraminifera biostratigraphy (more suitable for the shallow-marine Taleh Zang Formation) as late Danian, Selandian and Thanetian (~62–55.8 Ma) along the NE flank of the Amiran anticline. NP3, NP4 and NP5 biozones (Martini, 1971; Perch-Nielsen, 1981, 1985) are indeed very well documented in the Amiran Formation, whereas Thanetian levels contain characteristic *Taberina diavesi* and *Lockhartia diversa* foraminifera specimens (e.g. Smout, 1954; Pignatti *et al.*, 1998; see Homke *et al.*, 2009 for more details). The transition from the Taleh Zang to the Kashkan Formations is progressive. The base of the Kashkan Formation was therefore deposited during the Thanetian or the early Ypresian. Only one sample from the upper part of the Kashkan Formation has been successfully dated to the Ypresian (55.8–48.6 Ma) by palynostratigraphy. The base of the carbonates of the Shahbazan Formation, which cover the Kashkan conglomerates with a sharp contact, is dated as lowermost Oligocene at 33.9 ± 0.4 Ma by strontium isotope stratigraphy (Homke *et al.*, 2009). The three analysed samples provided consistent strontium isotope compositions that permitted to calculate ages using the LOWESS calibration from McArthur & Howarth (2004). The Ypresian age obtained for the upper part of the Kashkan Formation therefore suggests the presence of a protracted sedimentary hiatus between the Kashkan and the Shahbazan Formations in this region. The ~15 Myr hiatus encompasses most of the middle and upper Eocene and is characterized by either very slow sedimentation rates or nondeposition. Although more dating of the Kashkan Formation is required to support this hypothesis, it is well established that deposition of the Taleh Zang and Shahbazan Formations is separated by more than 20 Myr, during which only 320 m of preserved Kashkan deposits are recorded in this region (Homke *et al.*, 2009). The Shahbazan Formation may represent the distal part of a second foreland basin developed during the Oligocene, before the regional deposition of the Asmari Formation, as it is the case in the Fars for its equivalent Jahrom Formation (Mouthereau *et al.*, 2007).

Deposition of the evaporitic Gachsaran Formation marks a progressive return to continental conditions after deposition of the Asmari carbonate platform. The Gachsaran Formation is overlain by the second main detrital sequence of Miocene–Pliocene age, constituted by the Agha Jari and Bakhtyari Formations (Fig. 2). This detrital sequence was deposited in the Neogene foreland basin that preceded the present Mesopotamian basin. The Agha Jari Formation contains metamorphic, radiolaritic and calcareous material (James & Wynd, 1965) probably sourced from both the Imbricated Zone, including the Kermanshah ophiolitic units, and the Sanandaj-Sirjan Zone. Sparse paleocurrent directions towards the SE along the front of the Pusht-e Kuh Arc suggest that source areas for the Agha Jari Formation were mostly located to the NW of Lurestan Province and that rivers followed the axial foreland direction (e.g. Homke *et al.*, 2004; Vergés, 2007) (Fig. 1).

The Imbricated Zone

The Imbricated Zone to the NE of the Folded Belt represents the most external deformed sedimentary domain of the Arabian plate. It is made up of various tectonic units that were emplaced episodically over the NE Arabian margin during late Cretaceous and Cenozoic times. These are from bottom to top: (1) the radiolaritic–ophiolitic Kermanshah complex; (2) the magmatic and sedimentary Gaveh Rud domain; and (3) the thrust sheets carrying metamorphic rocks of the Sanandaj-Sirjan Zone (e.g. Braud, 1970; Agard *et al.*, 2005) (Fig. 3).

The radiolaritic–ophiolitic Kermanshah complex is composed from bottom to top by ~500–800-m-thick Triassic to Cretaceous radiolaritic series, the ~3000-m-thick Triassic to Cenomanian Bisotun platform and the relatively thin and discontinuous Coniacian–Santonian Harsin-Sahneh ophiolitic units (Fig. 3). The Harsin-Sahneh ophiolite was generated to the NE of the Bisotun platform around 85 Ma in an intraplate oceanic island arc environment (Delaloye & Desmons, 1980; Ghazi & Hassanipak, 1999). These ophiolites were subsequently emplaced and stacked on top of the Arabian platform domain as the Kermanshah tectonic slices. Thrust emplacement in the Imbricated Zone occurred from Santonian–Campanian to late Paleocene or early Eocene times (Berthier *et al.*, 1974; Gidon *et al.*, 1974; Braud, 1987), and initiated a flexural foreland basin, filled with the shallowing-upwards Amiran to Kashkan deposits (Fakhari & Soleimany, 2003; Alavi, 2004; Sherkati & Letouzey, 2004; Homke *et al.*, 2009).

The second main tectonic unit of the NW Imbricated Zone is the Gaveh Rud domain, also called Eocene domain by Agard *et al.* (2005) (Fig. 3). It represents a magmatic and sedimentary sequence possibly forming the forearc basin of the Sanandaj-Sirjan Arc. The Gaveh Rud domain consists from bottom to top of 700–800-m-thick Paleocene basaltic lavas, ~750 m of lower Eocene limestones and ~1500 m of Lutetian–Priabonian flysch deposits with Iranian affinity. This sequence is folded and cut by intrusions of gabbros of Bartonian age (40–34 Ma, Leterrier, 1985), which have been attributed to transpressive movements (Leterrier, 1985; Braud, 1987) or to detachment of the South Neo-Tethys subducting slab beneath the Sanandaj-Sirjan block (Agard *et al.*, 2005). Shortly after the Bartonian plutonic episode, the Gaveh Rud domain was tectonically transported over the radiolaritic–ophiolitic Kermanshah complex, sealed later by a thick deepening upwards sedimentary sequence of Oligocene–Miocene conglomerates, Aquitanian–Burdigalian carbonate platforms equivalent to the Asmari Formation and middle–late Miocene flysch deposits (Braud, 1987; Agard *et al.*, 2005).

The uppermost tectonic unit of the Imbricated Zone consists of thrust sheets carrying metamorphic rocks from the Sanandaj-Sirjan Zone over the middle–late Miocene flysch deposits (Fig. 3). To the SW, the basal thrust of this system cuts conglomerates, equivalent to the Bakhtyari Formation (Gidon *et al.*, 1974) and recently dated as Oligocene to early Miocene (~30–20 Ma) along the footwall of the Main Zagros Thrust (Fakhari *et al.*, 2008).

The Sanandaj-Sirjan Zone

The Sanandaj-Sirjan Zone, to the NE of the Imbricated Zone, forms a ~150–200-km-wide tectonic domain composed of deformed sedimentary and metamorphic Palaeozoic to Cretaceous rocks intruded by numerous Jurassic to late Eocene plutons (Alavi, 1994; Masoudi, 1997) (Fig. 1). The main metamorphic episode took place during the late Cretaceous, under greenschist and amphibolite conditions (Mohajjel & Fergusson, 2000). The Sanandaj-Sirjan Zone experienced a prolonged episode of calc-alkaline magmatism between the Jurassic and the end of the early Eocene (170–50 Ma), culminating during the late Cretaceous (e.g. Valizadeh & Cantagrel, 1975; Berberian & Berberian, 1981; Masoudi, 1997; Baharifar *et al.*, 2004). In NW Zagros, the Sanandaj-Sirjan Zone was moreover affected by intense gabbroic plutonism during Bartonian times (40–34 Ma) (Leterrier, 1985; Braud, 1987). The Sanandaj-Sirjan Zone shows NW–SE trending folds and thrust, which are south to SW directed.

The role of the Sanandaj-Sirjan Zone during the closure of the Neo-Tethys Ocean is still discussed. Despite the general assumption that this tectonic domain represents the southern edge of the Iranian plate (e.g. Berberian & King, 1981; Hooper *et al.*, 1994), distinct tectonic models

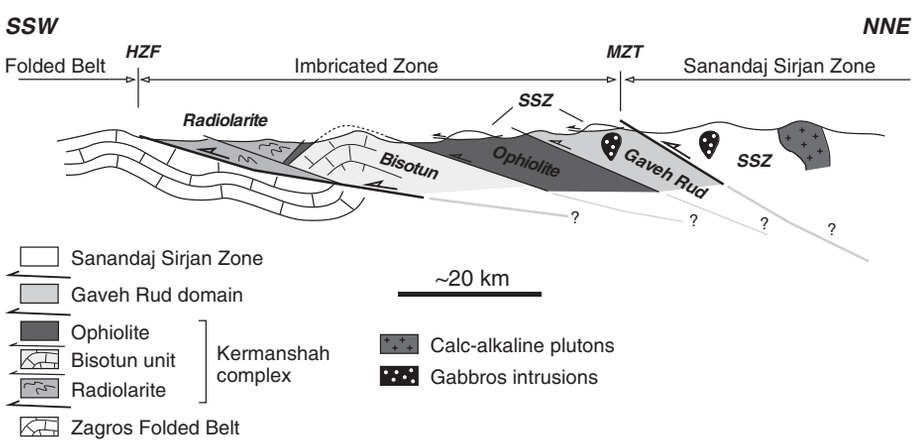

Fig. 3. Schematic cross-section summarizing the overall structure of the Imbricated Zone to the NE of the Pusht-e Kuh Arc. Simplified from Agard *et al.* (2005). HZF, high Zagros fault; MZT, main Zagros thrust; SSZ, Sanandaj-Sirjan thrust slices.

have been also proposed. Ghasemi & Talbot (2006) consider that the SE part of the Sanandaj-Sirjan Zone, which is bounded by ophiolites along both its SW and NE limits, was separated from the Iranian block by a distinct oceanic domain: the Maien-Baft oceanic realm of McCall (1999), whereas the NW part of the Sanandaj-Sirjan Zone remained attached to the Iranian plate. Alavi (1994) proposed a totally different model in which the entire Sanandaj-Sirjan Zone was part of the Arabian plate with its NE boundary representing the Zagros suture. Glennie (1995) interpreted the Sanandaj-Sirjan Zone as a small continental block that detached from the Arabian plate during opening of the South Neo-Tethys Ocean, and that was reaccreted to Arabia during its subsequent closure. According to Golonka (2004), the Sanandaj-Sirjan continental block separated from Arabia during opening of the South Neo-Tethys oceanic realm, and later drifted to the NE until its accretion to central Iran.

The Urumieh Doktar magmatic arc

The Tertiary Urumieh Doktar magmatic arc corresponds to a 50–100-km-wide tectonic domain located to the NE of the Sanandaj-Sirjan Zone (Fig. 1). This domain is generally regarded as an Andean-type magmatic arc formed on Iranian continental crust in response to northward subduction of the Neo-Tethys Ocean (e.g. Berberian *et al.*, 1982). Calc-alkaline magmatic activity started in the central part of the arc during the Eocene, and climaxed during Oligocene–Miocene times (Berberian & Berberian, 1981). Ages of dated intrusions range from 39 to 19 Ma (Bernard *et al.*, 1979; Martel-Jentin *et al.*, 1979; Berberian *et al.*, 1982; Bina *et al.*, 1986). According to Berberian & Berberian (1981), calc-alkaline magmatism ended around 5 Ma (early Pliocene), being replaced by alkaline volcanism in central Iran and SE Turkey. The most recent lavas of the Urumieh-Doktar magmatic arc are Quaternary in age (Alavi, 1994). The transition from calc-alkaline to alkaline volcanism is interpreted as resulting from slab break-off processes by several authors (e.g. Ghasemi & Talbot, 2006; Jahangiri, 2007).

FISSION-TRACK (FT) ANALYSES

Sampling

Samples were collected for apatite and zircon FT analysis from the two main well-dated detrital foreland sequences deposited in the NW Zagros, i.e. the late Maastrichtian–early Eocene Amiran–Kashkan sequence and the Miocene–Pliocene Agha Jari and Bakhtyari Formations. In addition, *in situ* metamorphic bedrock samples have been collected in the Sanandaj-Sirjan Zone (Fig. 4). Geographic coordinates and elevations of collected samples are reported in Table 1.

Bedrock samples

Bedrock samples have been collected in order to constrain the timing of exhumation experienced by the Sanandaj-Sirjan Zone just to the NE of the Pusht-e Kuh Arc. ive metamorphic samples have been collected in the Dorud metamorphic complex, which crops out in the NW Sanandaj-Sirjan Zone and culminates at 2396 m elevation (Figs 1 and 4a). The Dorud metamorphic complex is mostly composed of Permian to late Cretaceous deformed and metamorphosed (greenschist-amphibolite facies) sedimentary and magmatic rocks that are tectonically imbricated (Mohajjel & Fergusson, 2000). Three samples were collected in the central part of the complex (one diorite and two amphibolites), and two from its NE flank (gneiss from the Galeh Doz granite and amphibolite) (Fig. 4a, Table 1). However, only three of these samples yielded apatites and only two yielded some zircons (Fig. 5, Table 2).

Cobble samples from Bakhtyari conglomerates of the Kuh-e Farangui

Tectonic slices of the Sanandaj-Sirjan Zone including the Kuh-e Farangui thrust sheet (klippe) were emplaced over the Imbricated Zone and subsequently folded (Figs 1 and 4b). The Kuh-e Farangui tectonic unit overthrusts the lower part of the syntectonic Agha Jari and Bakhtyari deposits. The upper part of the Bakhtyari conglomerates, however, postdates thrust emplacement and is folded as a syncline together with the underlying thrust sheet. The upper levels of these conglomerates are generally considered to be Pliocene or younger (Gidon *et al.*, 1974; Braud, 1987; Agard *et al.*, 2005), although recent dating of presumed Bakhtyari conglomerates in the north of the Khuzestan Province suggests they may be as old as early Miocene in age (Fakhari *et al.*, 2008). One gneiss and two granite cobbles have been sampled from different stratigraphic levels along the 750-m-thick and 70°-dipping northern flank of the conglomeratic syncline (Fig. 6, Table 1). The three collected samples provided good quality apatites and few zircons (Fig. 6, Table 2).

Detrital samples from Paleocene Amiran–Kashkan foreland succession

The Amiran–Kashkan sequence, mostly derived from the Kermanshah radiolaritic–ophiolitic complex (James & Wynd, 1965; Alavi, 2004; Homke *et al.*, 2009), was sampled in central Lurestan along the NE flank of the Amiran anticline and the SW flank of the Sultan anticline (Fig. 4c). The Paleocene age of deposition of this succession has recently been determined by biostratigraphy (Homke *et al.*, 2009). In the Amiran anticline, nine samples have been collected from sandstone beds located at different levels of the 1225-m-thick sequence: five from the marine Amiran Formation, one from the shallow marine Taleh Zang Formation and three from the non-marine Kashkan Formation (Table 1). Only six of these samples yielded datable apatites. In the Sultan anticline, three samples were collected: two from the Amiran Formation and one from the basal layers of the Taleh Zang Formation. The three samples provided da-

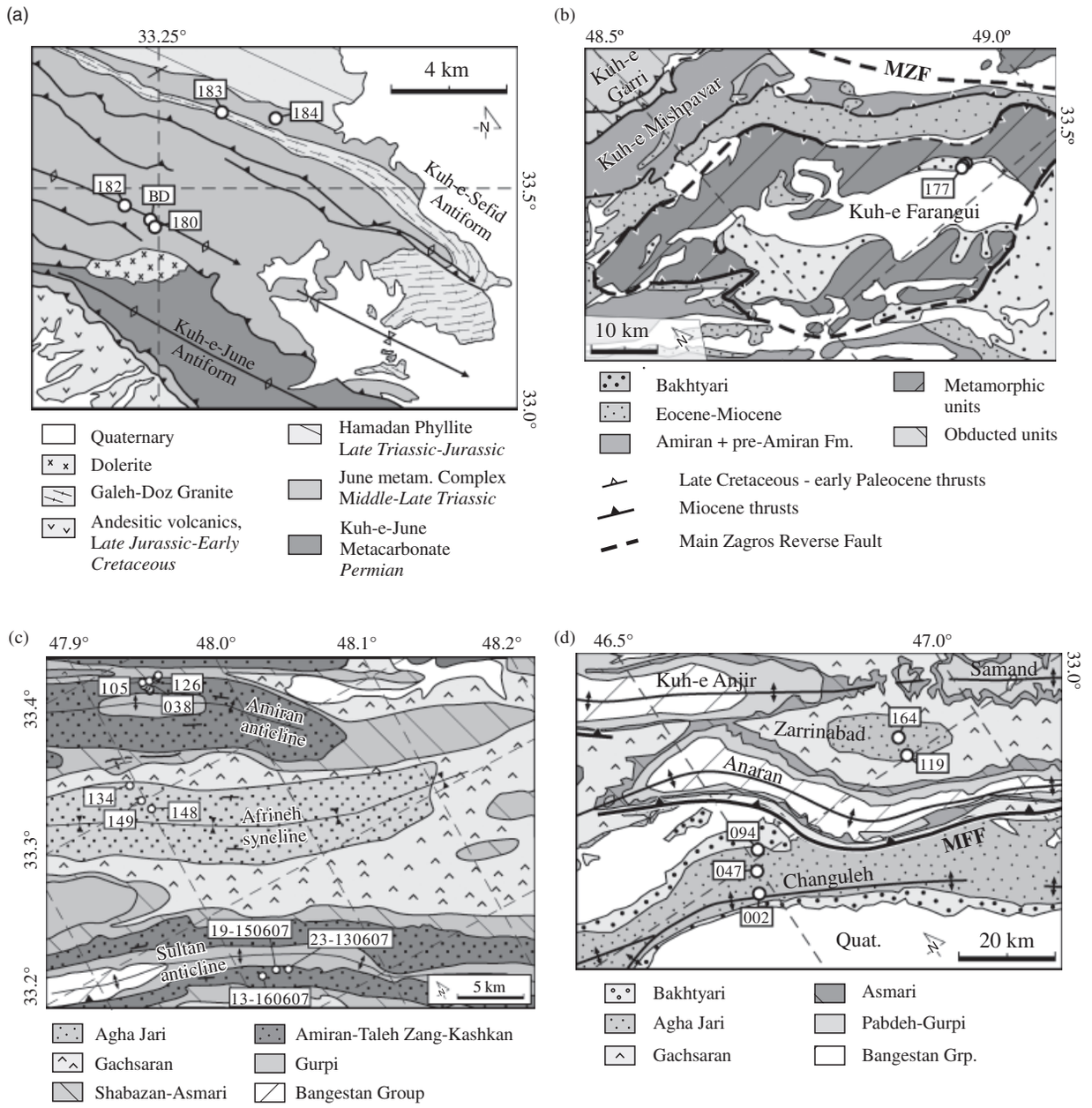

Fig. 4. Simplified geological maps of sampled areas (cf. Fig. 1 for location). Positions of samples are represented by white circles; sample references are given (see Table 1). (a) Geological map of the eastern termination of the Dorud metamorphic complex, in the Sanandaj-Sirjan Zone. (b) Geological map of the Kuh-e Farangui klippe, in the Imbricated Zone. (c) Geological map of the Amiran and Sultan anticlines and the Afrineh syncline. (d) Geological map of the frontal area of the Pusht-e Kuh arc. Samples were collected both in the Changuleh and the Zarrinabad synclines.

table apatites, but none of them contained zircons (Figs 7 and 8, Table 2).

Detrital samples from Miocene–Pliocene Agha Jari Formation

The fluvial Agha Jari Formation and the overlying conglomeratic Bakhtyari Formation fill the Mesopotamian foreland basin and are partially preserved in synclines of the Folded Belt (Fig. 1). Agha Jari sediments were mostly derived from the NE hinterland of the Zagros Belt (James & Wynd, 1965). Agha Jari deposits have been sampled in both the front of the Pusht-e Kuh Arc (Changuleh growth syncline and Zarrinabad syncline) and in its central part (Afrineh growth syncline, between the Amiran and Sultan anticlines) (Fig. 4c and d, Table 1). Three samples have been collected in the Changuleh syncline, two in the Zarrinabad syncline and three more samples in the Afrineh syncline (Figs 9 and 10, Table 1).

Experimental and analytical procedure

Sample preparation was performed in both the Laboratoire de Géodynamique des Chaînes Alpines, Université Joseph Fourier, in Grenoble (France) and the Servicio

Homologado de Termocronología, Universidad de Cádiz (Spain). Sample preparation and treatment followed standard techniques, as recently outlined by van der Beek *et al.* (2006). Apatite and zircon grains were separated from crushed rocks using classical sieving, heavy liquid and magnetic separation techniques. Apatite samples were mounted in epoxy resin and zircons in PFA Teflon. Mounted samples were then polished to expose an internal 4π surface. Apatite samples were etched in 5-mol HNO_3 at 20 °C for 20 s to reveal spontaneous tracks. Zircon samples were etched in a eutectic NaOH–KOH preparation (respectively, 11.5 and 8 g) at 230 °C. Apatite and zircon samples were irradiated separately in the Orphée reactor (CEA-Saclay, France). Thermal neutron fluence was monitored using NBS-962 glasses for apatites, and corning CN-1 glasses for zircons. The external detector method (muscovite slices) was used for analyses (Gleadow, 1981; Hurford & Green, 1982). Utilized muscovite slices were etched after irradiation in 40% HF acid at 20 °C for 20 min. Spontaneous and induced FTs were counted on an optical microscope with magnification of × 1000 dry objective. Central ages (Galbraith & Laslett, 1993) have been calculated with the zeta calibration method (Hurford & Green, 1983), using Durango (31.3 ± 0.3 Ma, Naeser & Fleischer, 1975) and Fish Canyon Tuff (27.8 ± 0.2, Hurford & Hammerschmidt, 1985) age standards. Confined track-length measurements were performed under a × 1000 dry objective, with a Kinetec automated Stage driven by FTStage software (Dumitru, 1993). Because of the common low number of observable confined FTs in each sample, we measured both tracks-in-track (TINT) and track-in-cleavage (TINCLE), despite their different response to etching (Barbarand *et al.*, 2003b). Orientation of FTs with respect to the *c*-axis of apatite grains controls both track annealing and etching rates (Donelick, 1991; Donelick *et al.*, 1999; Barbarand *et al.*, 2003a). The *c*-axis was therefore measured on analysed grains. Etch-pit widths parallel to *c*-axis (Dpar) were moreover measured for each dated apatite crystal, as they provide good assessment of annealing rate in individual apatite grains (e.g. Barbarand *et al.*, 2003a).

Table 1. Collected apatite fission-track (AFT) samples

Sampling site	Sample	Easting (m)	Northing (m)	Elevation (m)	AFT
Dorud complex	SHBD	338 139	3 715 547	2078	X
	SH180	338 567	3 715 094	2123	X
	SH182	334 921	3 716 866	1870	O
	SH183	340 007	3 719 987	2124	O
	SH184	344 968	3 718 822	2042	O
Kuh-e Farangui	SH177	297 239	3 713 637	1965	O
	SH178	297 710	3 713 803	1994	O
	SH179	298 199	3 713 921	2038	O
Amiran anticline	SH137	775 480	3 698 077	904	X
	SH133	775 417	3 698 028	904	X
	SH126	775 272	3 697 894	904	O
	SH116	774 466	3 698 091	1008	O
	SH105	773 972	3 698 221	1075	O
	SH084	774 061	3 698 034	7037	O
	SH061	774 170	3 697 773	993	O
	SH038	774 478	3 697 391	937	O
	SH013	774 592	3 697 107	914	X
Sultan anticline	SH13-07	771 563	3 673 733	1140	O
	SH19-07	772 174	3 674 068	1182	O
	SH23-07	773 572	3 673 830	1188	O
Afrineh syncline	SH148	769 005	3 689 363	849	O
	SH149	769 280	3 690 224	827	O
	SH144	769 734	3 691 632	877	X
Changuleh syncline	SH094	641 114	3 654 962	297	O
	SH047	639 676	3 651 879	201	O
	SH002	636 334	3 649 362	200	O
Zarrinabad syncline	SH164	672 220	3 659 304	757	O
	SH119	673 078	3 653 437	700	X

Coordinates (UTM38-N) and altitudes are in meters. Samples that did not yield apatite are marked by an X.

Mixed grain-age distributions were decomposed by the binomial peak-fitting method into grain-age components defined by an estimated age and size (Galbraith & Green, 1990; Brandon, 1992; Galbraith & Laslett, 1993; Stewart & Brandon, 2004). Peak-fitting analysis for detrital samples with a low number of dated crystals may provide unreliable results. In order to obtain more information about cooling ages, combined grain-age distributions of several detrital samples from the Agha Jari Formation have been analysed, provided that these samples did not record different degrees of partial annealing.

Thermal history modelling was carried out for three samples with the program AFTSolve® version 1.4.1 (Ketcham *et al.*, 2000), in which the multi-kinetic annealing model of Ketcham *et al.* (1999) was applied, using Dpar as

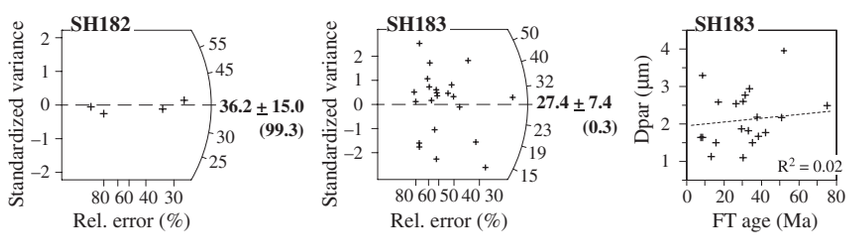

Fig. 5. Radial plots of dated samples from the Dorud metamorphic complex (Fig. 4a). Central ages are given in bold numbers with χ^2 probability (%) in brackets. Dpar vs. fission-track (FT) age plot is given for sample SH183. The low value of the linear regression parameter R^2 indicates absence of a clear relationship between Dpar and FT ages.

Table 2. Apatite fission track analytical data

Sample	Formation	Stratigr. level (m)	Deposition age	No. of grains	ρ_s (N_s) $\times 10^5$ cm^{-2}	ρ_i (N_i) $\times 10^5$ cm^{-2}	ρ_d (N_d) $\times 10^5$ cm^{-1}	$P(\chi^2)$ (%)	Disp. (%)	Central age+2σ (Ma)	No. of lengths	Mean TL+ 1σ (μm)	SD (μm)	No. of Dpar	Mean Dpar (μm)	SD (μm)
Dorud complex																
SH183	Gneiss	–	Cretaceous	22	2.361 (149)	10.156 (641)	6.818 (17 684)	0.3	38	27.4 ± 7.4	–	–	–	94	1.81	0.67
SH184	Amphibolite	–	Metamorphism	3	3.090 (15)	6.797 (33)		25.3	0	47.8 ± 30.0	–	–	–	8	1.38	0.29
SH182	Amphibolite	–		4	5.467 (33)	15.904 (96)		99.3	0	36.2 ± 15.0	–	–	–	13	1.49	0.50
Kuh-e Farangui conglomerates																
SH177	Granite	750	Pleistocene	24	18.439 (519)	43.060 (1212)		99.9	0	45.1 ± 6.2	50	13.1 ± 0.3	1.9	119	1.68	0.45
SH178	Granite	523		26	19.701 (804)	52.831 (2156)	6.818 (17 684)	99.8	0	39.3 ± 4.8	74	13.2 ± 0.2	1.6	146	1.45	0.31
SH179	Gneiss	315		25	1.382 (101)	3.270 (239)		92.5	9	45.1 ± 11.6	6	12.6 ± 0.7	1.7	41	1.43	0.38
Amiran anticline																
SH126	Kashkan	996	56.8 ± 1.7	51	1.502 (332)	2.958 (654)	6.818 (17 684)	98.6	5	53.5 ± 8.8	14	13.2 ± 0.5	1.9	109	2.75	1.13
SH116	Taleh Zang	890	57.2 ± 1.5	43	1.280 (319)	2.544 (634)		99.7	0	52.9 ± 8.8	6	13.0 ± 0,4	0.9	94	2.74	0.91
SH105	Amiran	795	57.6 ± 1.3	23	1.122 (128)	1.876 (214)		97.8	0	62.9 ± 15.2	3	10.8 ± 0.6	1.0	72	2.61	1.00
SH084	Amiran	631	58.2 ± 1.0	6	2.369 (30)	4.264 (54)		99.8	0	58.4 ± 27.2	2	10.3 ± 2.1	2.9	24	2.89	1.39
SH061	Amiran	444	58.9 ± 0.5	29	2.381 (294)	5.199 (642)		98.5	0	48.2 ± 8.0	11	11.4 ± 0.7	2.3	103	3.02	1.09
SH038	Amiran	256	59.6 ± 0.3	47	1.100 (275)	2.631 (658)		98.7	0	44.0 ± 7.4	33	11.7 ± 0.3	2.0	119	1.97	0.68
Sultan anticline																
SH13-07	Amiran	884	Ypresian	49	4.57 (996)	12.00 (2608)	13.50 (6529)	0.0	42	79.8 ± 6.4	9	13.3 ± 0.4	1.2	113	4.29	1.7
SH19-07	Amiran	390	Thanetian	39	2.80 (435)	8.02 (1246)	13.33 (6179)	0.0	39	76.8 ± 6.9	18	12.2 ± 0.6	2.7	146	3.91	1.6
SH23-07	Amiran	156	Thanetian	56	4.41 (1034)	9.41 (2206)	13.15 (6098)	0.0	70	110.2 ± 8.9	8	12.4 ± 0.4	1.2	188	3.37	1.6
Afrineh syncline																
SH148	Agha Jari	877	Miocene	22	3.076 (341)	13.431 (1489)	6.818 (17 684)	9.6	20	24.2 ± 4.2	12	13.1 ± 0.5	1.8	97	2.29	0.66
SH149	Agha Jari	525	Miocene	23	3.856 (258)	11.792 (789)		7.0	24	35.5 ± 7.2	7	13.5 ± 0.3	0.8	86	1.61	0.50
Changuleh-Zarrinabad area																
SH094	Lahbari Mb.	2482	5.4 ± 0.1	30	8.757 (995)	18.923 (2150)	5.722 (11 674)	0.0	29	48.5 ± 6.8	–	–	–	–	–	–
SH047	Bakhtyari	1600	2.6 ± 0.1	19	6.265 (619)	14.514 (1434)		0.0	46	48.6 ± 12.2	–	–	–	–	–	–
SH002	Agha Jari	850	9.0 ± 0.1	27	7.392 (725)	14.518 (1424)		0.0	34	53.4 ± 9.0	–	–	–	–	–	–
SH164	Agha Jari	825	9.2 ± 0.1	31	5.950 (825)	13.726 (1903)		0.2	21	43.0 ± 5.2	–	–	–	–	–	–

ρ_s and N_s, density and number of spontaneous fission tracks, respectively. ρ_i and N_i, density and number of induced fission tracks. ρ_d and N_d., density and number of measured in fluence dosimeter. Sultan anticline samples have been analysed by L. Barbero. Other samples have been analysed by S. Homke. ζ for samples from Changuleh and Zarrinabad is 341.1 ± 5.3, with dosimeter NBS962/612. ζ for samples from Sultan anticline is 339.0 ± 5.0 with dosimeter CN-5. ζ for other samples is 309.8+13.8, with dosimeter NBS962/612. P(χ2), chi-squared probability that grain ages are concordant. Disp., age dispersion. A sample may contains multiple age populations if $P(\chi^2) < 5$ and/or Disp > 15 (Galbraith & Green, 1990; Galbraith & Laslett, 1993). SD, standard deviation of mean confined track length and mean Dpar (μm).

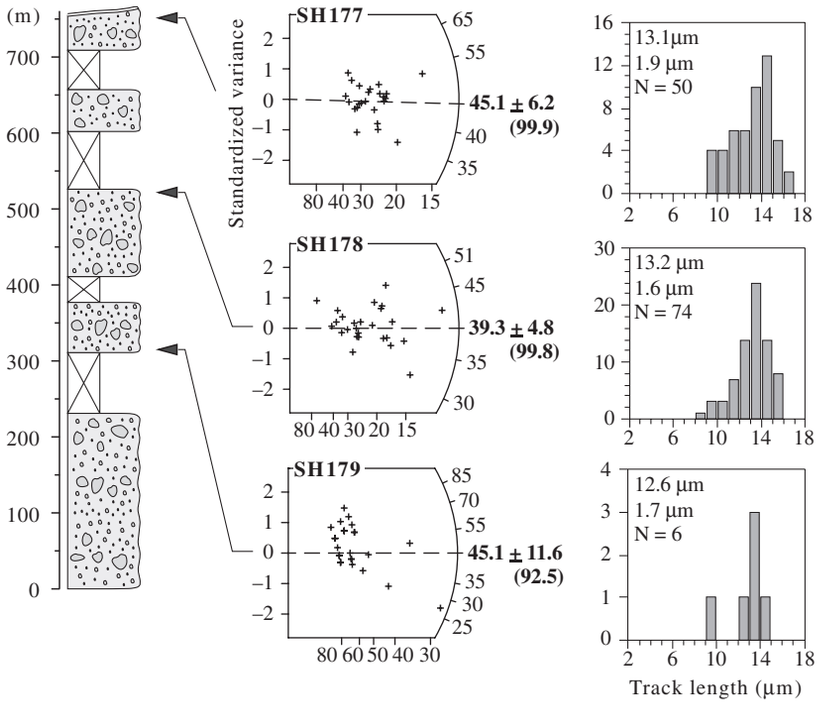

Fig. 6. Stratigraphic column and fission-track sampling of Pliocene conglomerates covering the Kuh-e Farangui klippe (Fig. 4b). Radial plots are given with central ages age in bold and χ^2 probability (%) in brackets. Track lengths histograms of dated samples are given with mean length, standard deviation and number of measured tracks.

kinetic variable (Carlson *et al.*, 1999; Barbarand *et al.*, 2003a). The effect of crystallographic orientation of measured confined tracks was corrected using the *c*-axis projection method of Donelick *et al.* (1999). The Kolmogorov–Smirnov test (KS) was used to compare measured FT length distributions to track-length distributions predicted by the models and the goodness-of-fit test (GOF) was used to compare age data with modelled ages (Ketcham *et al.*, 2000). Envelopes of statistically 'acceptable' *t*—*T* paths (with KS and GOF value both higher than 0.05) and of 'good' *t*–*T* paths (with KS and GOF value both higher than 0.5) are calculated by the program for each model run (Ketcham *et al.*, 2000). For each sample, three runs have been performed using the Monte Carlo search method with 50 000 steps and with different *T*–*t* constraints. Obtained confidence envelopes are combined for each sample to build more complete confidence envelopes. Moreover, Constrained Random Searches with 50 000 iterations have been performed to find best-fit solutions (Ketcham *et al.*, 2000).

RESULTS

On average, our samples yielded relatively few apatite and insufficient zircon grains. Reliable AFT results have, however, been obtained for several detrital and metamorphic samples. All ages reported are central ages (Galbraith & Laslett, 1993) with $\pm 2\sigma$ error.

Dorud metamorphic complex

The five samples collected in the Dorud metamorphic complex in the Sanandaj-Sirjan Zone (Fig. 4a) had very low yield. Only three samples contained datable apatite grains (SH182–SH184), two of them providing only three and four datable grains (Fig. 5, Table 2). No confined FT lengths could be measured in the three dated samples.

Four measured apatite grains of amphibolite sample SH182 provided concordant individual FT ages, with a central age of 36.2 ± 15.0 Ma (Fig. 5, Table 2). A gneiss sample (SH183) from the deformed Galeh Doz granite on the NE flank of the Dorud metamorphic complex provided 22 datable apatite grains with a central AFT age of 27.4 ± 7.4 Ma. Great age dispersion (38%) and very low χ^2 probability (0.3%) suggest prolonged residence in the Partial Annealing Zone (PAZ) (Fig. 5, Table 2). Spreading of individual grain ages may result from different chemical compositions of the apatites, although there is no clear correlation between Dpar values and FT ages (Fig. 5). An amphibolite sample (SH184) provided only three apatite crystals, with individual FT ages of 0 (no fossil tracks), 40 and 105 Ma (Table 2). Because of the low number of apatites and the large difference in individual FT ages, the central FT age (48 ± 30 Ma) of this sample is not considered reliable for interpretation.

Kuh-e Farangui thrust sheet

The gneiss and granite cobbles collected in the folded conglomerates on top of the Kuh-e Farangui thrust sheet (Fig. 4b) provided numerous good-quality apatite grains. Concordant FT ages have been obtained for these samples, with χ^2 probability >92.5%, at 45.1 ± 11.6 (SH179), 39.4 ± 4.8 (SH178) and 45.1 ± 6.2 Ma (SH177) (Fig. 6, Table 2). 50 and 74 confined tracks were measured in the two granite samples SH177 and SH178, respectively. Track-length distributions of these samples are characterized by

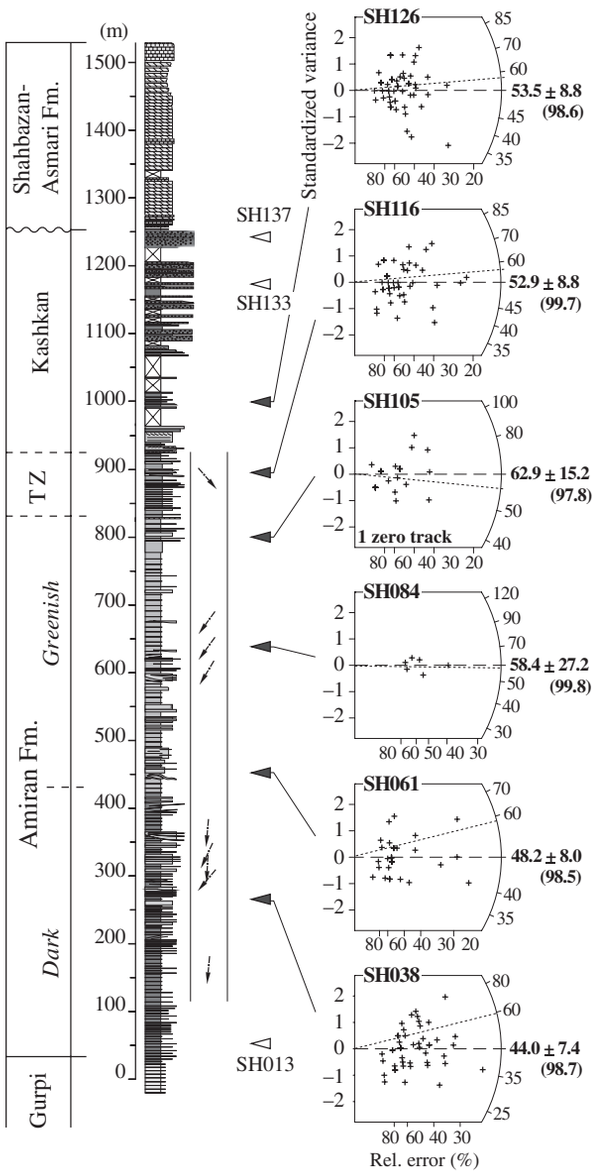

Fig. 7. Stratigraphic column of the Amiran–Kashkan detrital sequence and the overlying Shahbazan-Asmari Fm. in the Amiran anticline (cf. Fig. 4c for location). Small black arrows represent measured paleocurrent directions (Homke *et al.*, 2009). Positions of collected AFT samples are indicated by triangles (white for undatable samples). Radial plots of successfully dated samples are given. Central ages are in bold with χ^2 probability (%) in brackets. Dot lines represent deposition ages.

means of 13.1 and 13.2 μm, standard deviations of 1.9 and 1.6 μm and the presence of confined tracks < 10 μm long (Fig. 6, Table 2).

Amiran Formation – Amiran anticline

Six apatite samples collected in the NE flank of the Amiran anticline (Fig. 4c) have been successfully dated. Four samples were collected in the Amiran Formation, one in the Taleh Zang Formation and one from the lower part of the Kashkan Formation (Fig. 7, Table 2). High χ^2 probability ($> 97\%$) and low age dispersion ($< 5\%$) indicate that all samples contain single grain-age populations. This is consistent with a unique sedimentary source derived from the ophiolitic–radiolaritic Kermanshah complex (Homke *et al.*, 2009). Apatite may come from mafic igneous rocks that mainly form the Harsin-Shaneh ophiolite (Ghazi & Hassanipak, 1999). The least constrained central age has been obtained for sample SH084, with only six dated apatite grains. Other samples provided between 23 (SH105) and 51 (SH126) grains (Fig. 7, Table 2).

AFT ages are younger than depositional ages, and they generally decrease with depth (Fig. 11a and b). This indicates that AFT ages have been partially reset due to burial of the foreland succession. As discussed in Homke *et al.* (2009), fluid circulation and associated advective heat transport across the foreland basin could produce significant reheating of sediments and be the cause for the greenish colouration and major remagnetization of the upper-half part of the Amiran Formation, as well as partial resetting of the AFT ages in this region. Similar changes have been detected in other foreland basins, among which the western Canada and South Pyrenean basins (e.g. Ravenhurst *et al.*, 1994; Juez-Larré & Andriessen, 2006; Travé *et al.*, 2007; Gong *et al.*, 2008).

Relatively few track lengths have been obtained, with a maximum of 33 measurements for sample SH038 (Table 2), because of low uranium content (< 11 p.p.m.). Mean track lengths generally decrease down section, with an average of 11.7 μm for sample SH038 (Table 2), consistent with partial annealing.

Amiran Formation – Sultan anticline

Three detrital samples collected in the SW limb of the Sultan anticline contained datable apatite grains (Fig. 4c). Stratigraphic ages of the Sultan anticline are comparable to or slightly younger than those of the Amiran anticline succession (Fig. 11b and c). A sedimentary hiatus or a condensed level in the basal part of the Sultan section, in the top of the Gurpi Formation, is evidenced by the lack of nannoplankton biozones NP1 and NP2. The Paleocene–Eocene boundary is located somewhat below the transition between the Amiran and Taleh Zang Formations ($\sim$770 m), as indicated both by calcareous nannoplankton and large foraminifera content. Finally, the contact between Kashkan and Shahbazan Formations is also characterized by a sedimentary hiatus or slowing of deposition with a duration that may reach about 15 Myr, as demonstrated by the strontium-isotope ages calculated for the base of the Shahbazan Formation (Homke *et al.*, 2009).

The three analysed samples failed the χ^2 test and present age dispersions between 42% and 70%, suggesting the presence of mixed grain-age populations (Fig. 8, Table 2). Sample SH23-07 has been decomposed into three grain-age populations of different sizes, with age peaks at 17.0 ± 15.9, 87.8 ± 10.2 and 224.9 ± 40.4 Ma. These ages are only roughly constrained due to the reduced number of

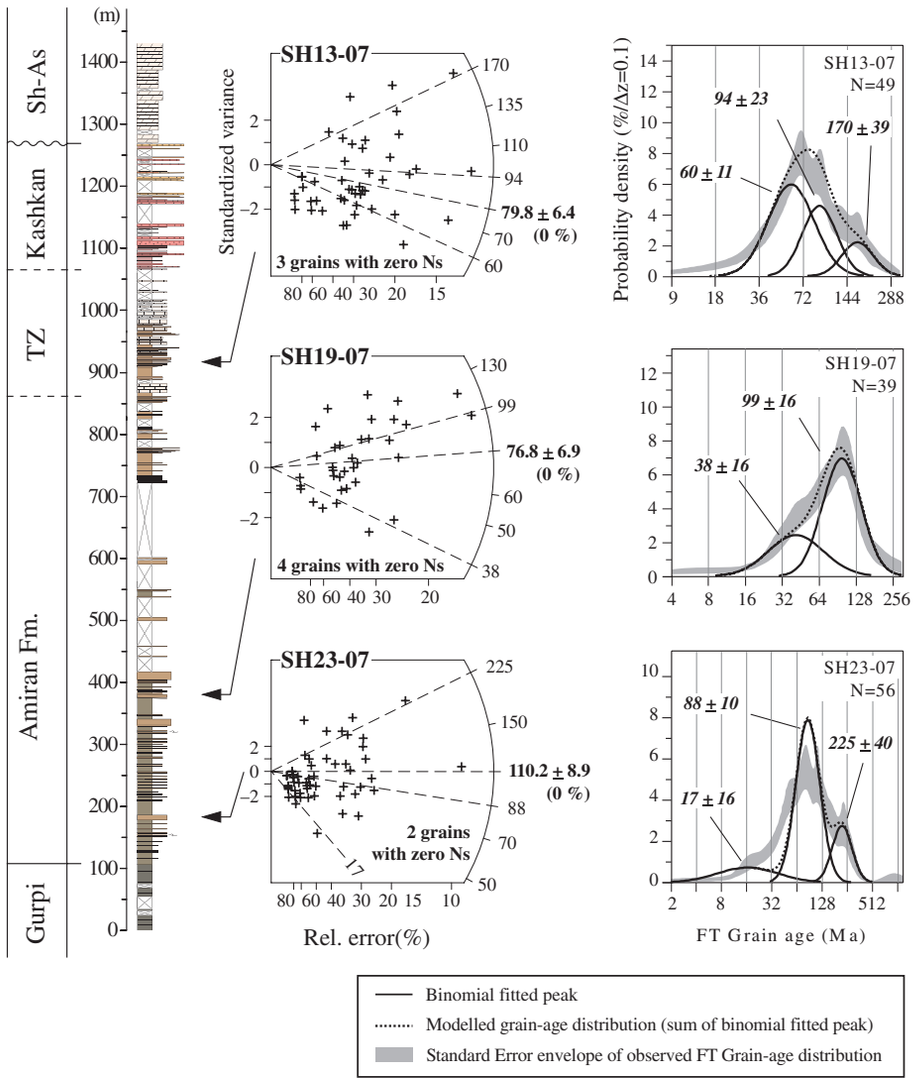

Fig. 8. Stratigraphic column of the Amiran–Kashkan detrital sequence and the overlying Shahbazan-Asmari Fm. in the Sultan anticline (cf. Fig. 4c for location). Positions of collected AFT samples are indicated by triangles. Radial plots and grain-age probability density plot with binomial fitted peaks are given. Central ages in bold, with χ^2 probability (%) in brackets.

crystals and high age variability. Sample SH19-07, provided age peaks at 38.4 ± 15.8 and 98.5 ± 15.8 Ma. Sample SH13-07 also provided three grain-age populations, with age peaks at 59.9 ± 10.7, 93.6 ± 22.8 and 170.5 ± 39.4 Ma (Fig. 8, Table 3).

As in the Amiran anticline, the ages of youngest identified grain-age components decrease with depth and are close to or younger than depositional ages. This indicates that samples from the Sultan anticline have also been partially annealed due to burial and potential fluid circulation (Fig. 11). However, they are characterized by significantly higher mean Dpar values than those from the Amiran anticline and thus appear less annealed, explaining why they retain pre-Tertiary age peaks whereas samples from the Amiran anticline do not.

Agha Jari Formation – Afrineh growth syncline

Two of the three samples collected in the lower 850 m of the Miocene–Pliocene Agha Jari Formation preserved in the Afrineh growth syncline (Fig. 4c) contained datable apatite grains (Fig. 9, Table 2). Both samples failed the χ^2 test and show age dispersion of 20% and 24%, respectively, revealing the presence of mixed grain-age components. FT grain-age distributions of both samples can be decomposed in two grain-age components of roughly equal size. The age peaks of these components are 19.6 ± 5.5 and 31.3 ± 9.8 Ma for sample SH148, and 26.3 ± 10.3 and 46.4 ± 15.8 Ma for sample SH149 (Fig. 9, Table 3), although none of these ages are very well constrained because of the low number of dated apatites (22 and 23 grains). χ^2 probabilities of best fitted binomial components are <20% (Table 3). The two dated samples were collected from the uppermost part of the sedimentary cover, and they were not buried sufficiently to be partially annealed since deposition (Fig. 11). The decomposition of combined grain-age distributions (45 grains) was performed to limit problems due to the low number of grains and because of the overlap of age peaks. Two grain-age components of equivalent size, with estimated age of 21.5 ± 5.3 and 37.4 ± 9.8 Ma were obtained with a χ^2 probability of 42.3%, which is more

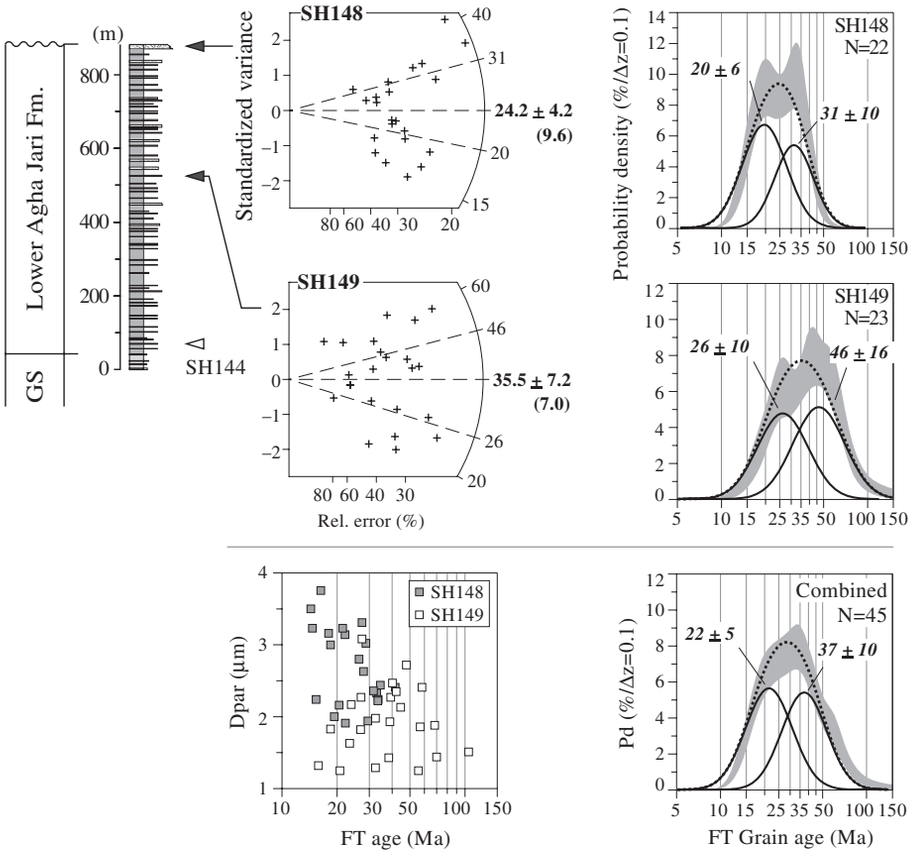

Fig. 9. Stratigraphic column of the lower Agha Jari Fm. preserved in the Afrineh syncline (Fig. 4c). Positions of collected apatite fission-track (AFT) samples are indicated by triangles (white for undatable sample). Radial plots and grain-age probability density plots of the two successfully dated samples are given. Combined probability density plot is also shown (see Fig. 8 for legend). Dpar of dated apatites are plotted vs. individual calculated fission-track (FT) ages.

reliable than the fit for the individual samples (Fig. 9, Table 3).

Both age peaks were apparently not partially reset after sample deposition, and they probably indicate source-area denudation ages (Fig. 11a, Table 3). The absence of correlation between Dpar (i.e. chemical composition) and single-grain ages (oldest AFT ages are represented by the least resistant apatites with low Dpar values) is consistent with this interpretation (Fig. 9).

Agha Jari Formation – Zarrinabad and Changuleh growth synclines

Four samples collected in the Zarrinabad and Changuleh growth synclines at different levels of the Agha Jari and lowermost Bakhtyari Formations yielded datable apatite grains (Fig. 10, Table 2). Discordant grain-age distributions of studied samples, with χ^2 probability $<0.2\%$ and age dispersion between 21%, and 46%, reveal the presence of mixed grain-age components. For each sample, two grain-age populations have been identified. Because of the relatively low number of dated apatites (between 19 and 31 grains), these grain-age populations are not very well constrained and additional less important grain-age populations may not have been recovered. All samples, however, display a similar dominant component with mean age ranging from 33.7 ± 4.1 (SH047) to 40.1 ± 3.9 Ma (SH094). The age distribution of the second population ranges from 61 ± 17.7 (SH164) to 94.6 ± 22.9 Ma (SH047). χ^2 probability of best-fitted peaks ranges from 16.0% to 29.6% (Fig. 10, Table 3).

Sample SH047, which was deposited during folding in front of the belt, and which probably experienced <1 km of burial, is not considered to be significantly thermally annealed. Samples SH164 and SH002 may have entered the PAZ during deposition of the upper part of the Agha Jari–Bakhtyari succession, with a maximum burial of $\sim$2 km (Fig. 10). However, it is probable that these samples, deposited slightly before the onset of folding in the front of the belt, spent only a limited time in the PAZ before final exhumation during amplification of folding. Overlap of the main age peaks of the four analysed samples suggests that thermal annealing of these two lower samples is minor. Therefore, decomposition of the combined grain-age distribution (107 grains) was performed in order to obtain a better definition of dominant grain-age populations. Three grain-age populations were differentiated, one prominent population with a peak age at 37.6 ± 2.6 Ma (68.3%), and two minor populations with peak ages at 66.3 ± 29.8 Ma (14.0%) and 90.8 ± 17.7 Ma (21.3%) (Fig. 10, Table 3). The significance of the two older populations may be questioned because of their important age uncertainty.

Thermal history modelling

Modelling of individual thermal histories of granite samples SH177 and SH178, both from large cobbles from the Bakhtyari conglomerates overlapping the Kuh-

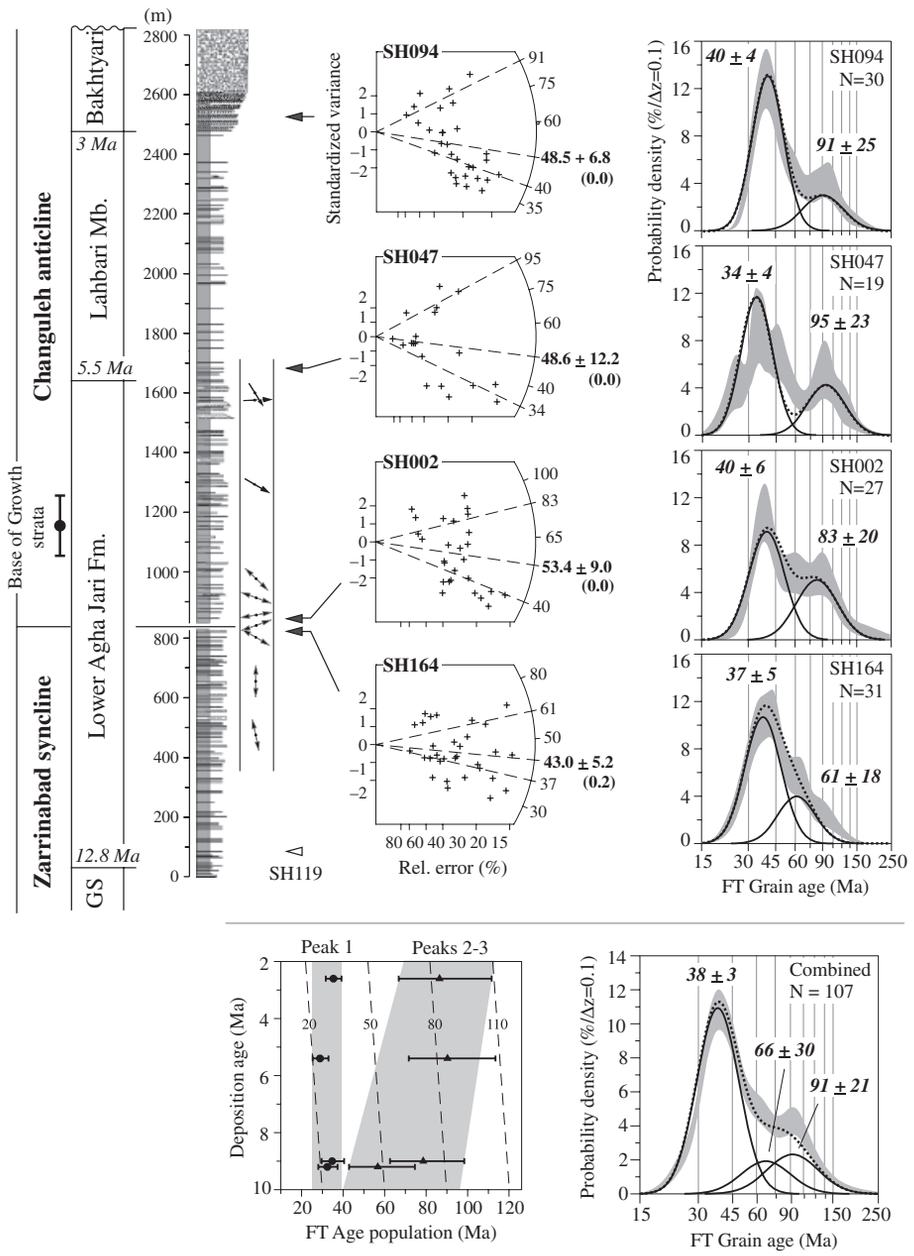

Fig. 10. Synthetic stratigraphic column of Agha Jari and Bakhtyari Formations studied along the Zarrinabad syncline and the Changuleh anticline, in the MFF area (Fig. 4d). Age of formations, channel orientations and the base of growth strata are given (Homke *et al.*, 2004). Collected apatite fission-track (AFT) samples are located in the column. Grain-age probability–density plots of the four successfully dated samples, and of their combined apatite populations, are given (see the Fig. 8 for the legend). Stratigraphic age vs. AFT age plot is also represented.

e Farangui thrust sheet (Figs 4b and 12) have been carried out; 74 and 50 confined track-length measurements were available for samples SH177 and SH178, respectively. No clear correlation appears between *c*-projected track lengths and Dpar values (Fig. 12). Moreover, because few track-length measurements are available, it was not possible to define multiple kinetic populations for thermal history modelling of these samples. We therefore used a single kinetic population based on Dpar values for each sample.

Results suggest relatively slow cooling through time. According to the modelling, sample SH178 (Fig. 12a) probably entered the PAZ (Gleadow & Fitzgerald, 1987; Brown *et al.*, 1994) in early Eocene times, and exited it in early Miocene times. The cooling rate of sample SH178 averaged $\sim 5\ ^{\circ}\mathrm{C\ Myr^{-1}}$ until late Eocene times, and may have decreased afterwards to $\sim 1\ ^{\circ}\mathrm{C\ Myr^{-1}}$. Sample SH177 (Fig. 12b) probably entered the PAZ during the late Paleocene, and exited it in early Miocene times, showing a similar linear overall cooling history to sample SH178. Although results have been obtained with GOF and KS statistics > 0.95, the relatively low number of track-length measurements, in particular for sample SH177, as well as the use of a single kinetic population for modelling, reduces our confidence in the model predictions and thus given cooling rates are only indicative (Fig. 12).

DISCUSSION

Five families of AFT ages and grain-age populations have been obtained from both detrital (Amiran and Agha Jari

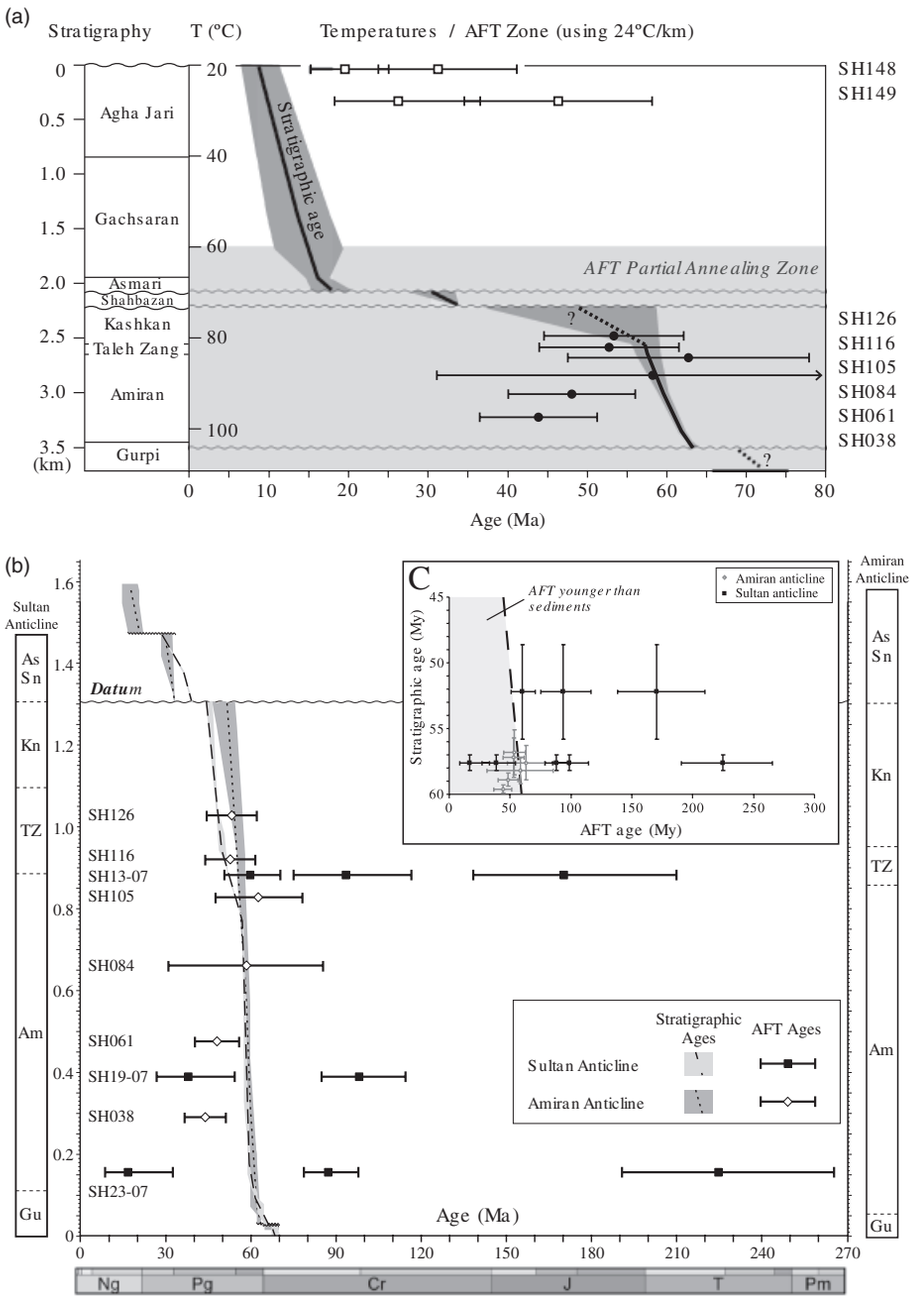

Fig. 11. (a) Apatite fission-track (AFT) age vs. stratigraphic position of Amiran–Kashkan detrital samples (black circles) and Agha Jari detrital samples (white squares) collected in the Afrineh syncline (Figs 4c, 7 and 9). Central ages are plotted for samples with a single age population and individual age peaks for those with multiple populations. Stratigraphic ages are presented with approximate confidence limit. Temperatures are calculated using a stable geothermal gradient of 24 °C km^{-1} and a surface temperature of 20 °C. This corresponds to the situation in the Amiran basin around 9 Ma, and to the present-day situation in the Afrineh syncline. (b) Stratigraphic and AFT ages vs. thickness of the Amiran–Kashkan succession in the Amiran (black squares) and Sultan (white diamonds) anticlines. As-Sn, Asmari-Shabazan; Kn: Kashkan; TZ, Taleh Zang; Am,: Amiran; Gu, Gurpi. (c) AFT ages vs. stratigraphic ages in the Amiran and Sultan anticlines.

deposits) and crystalline samples: (1) pre-middle Jurassic (~171, ~225 Ma); (2) early–late Cretaceous (~91 Ma); (3) Maastrichtian (~66 Ma); (4) middle–late Eocene (~38 Ma); and (5) late Oligocene to early Miocene (~22 Ma) (Figs 5–10). Although some these ages may result from partial annealing, they provide indications of distinct cooling/denudation episodes that occurred in the inner zones of the present NW Zagros, i.e., the Imbricated Zone and the Sanandaj-Sirjan Zone (the most probable source areas for the Amiran and Agha Jari–Bakhtyari deposits). The potential large scale of some of these denudation events, documented by AFT ages, in the inner Zagros may have influenced the foreland basin evolution as depicted in Fig. 13.

Pre-Eocene cooling

The oldest identified AFT grain-age populations, at 171 ± 39 and 225 ± 40 Ma, were encountered in detrital samples of the Amiran and Taleh Zang Formations in the Sultan anticline. These ages are probably partially reset, and are thus difficult to directly interpret as cooling ages, although they may record a pre-Jurassic tectonic event possibly related to the late Triassic closure of the Paleo-Tethys realm (Berberian & Berberian, 1981; Horton *et al.*, 2008) (Fig. 13). The fact that these detrital apatites were deposited in the Paleocene Amiran foreland basin suggests a proximal source for them, with a potential origin in the tectonic slices derived from the NE margin of the Arabian

Table 3. Results of binomial peak-fitting

Sample		Formation	Stratig. level (m)	Deposition age	No. of grains	Population 1			Population 2			Population 3			$P(\chi^2)$
						Peak	CI (95%)	Frac (%)	Peak	CI (95%)	Frac (%)	Peak	CI (95%)	Frac (%)	
Afrineh syncline															
1	SH148	Agha Jari	879	Miocene	22	19.6	−4.3/+5.5	58.9	31.3	−7.5/+9.8	41.1	–	–	–	15.8
2	SH149	Agha Jari	525	Miocene	23	26.3	−7.4/+10.3	47.7	46.4	−11.8/+15.8	52.3	–	–	–	18.2
3	Combined	(1+2)	–	–	45	21.5	−4.3/+5.3	52.2	37.4	−7.7/+9.8	47.8	–	–	–	42.3
Changuleh-Zarrinabad area															
4	SH094	Lahbari Mb.	2482	5.4 ± 0.1	30	40.1	−3.6/+3.9	77.0	90.8	−19.5/+24.9	23.0	–	–	–	25.4
5	SH047	Bakhtyari	1600	2.6 ± 0.1	19	33.7	−3.5/+4.1	69.4	94.6	−18.5/+22.9	30.6	–	–	–	16.0
6	SH002	Agha Jari	850	9.0 ± 0.1	27	39.5	−5.0/+5.7	60.8	83.0	−15.9/+19.6	39.2	–	–	–	26.0
7	SH164	Agha Jari	825	9.2 ± 0.1	31	37.2	−4.3/+4.9	22.3	61.3	−13.7/+17.7	8.7	–	–	–	29.6
8	Combined	(4+5+6+7)	–	–	107	37.6	−2.4/+2.6	68.3	66.3	−20.6/+29.8	14.0	90.8	−17.3/+21.3	17.7	96.3
Sultan anticline															
9	SH13-07	Amiran	884	Ypresian	49	59.9	−9.1/+10.7	54.6	93.6	−18.4/+22.8	31.4	170.5	−32.1/+39.4	14.0	55.3
10	SH19-07	Amiran	390	Thanetian	39	38.4	−11.2/+15.8	35.9	98.5	−13.6/+15.8	64.1	–	–	–	39.4
11	SH23-07	Amiran	156	Thanetian	56	17.0	−8.2/+15.9	15.3	87.8	−9.1/+10.2	65.5	224.9	−34.3/+40.4	19.2	61.8

$P(\chi^2)$: chi-squared probability that the obtained age peaks represent the measured fission track grain age (FTGA) population; Peak: mean age of the peak, in Ma; CI, (95%): confidence interval (at 95%) of calculated mean age; Frac (%): estimated relative peak size (%) in the FTGA population.

plate, imbricated and exhumed as a consequence of late Cretaceous oceanic obduction.

Overlapping age peaks around 91–98 Ma in samples SH094, SH047 and SH002 (detrital apatites in the Agha Jari Formation) may correspond to apatites sourced from magmatic rocks related to the ophiolites of the Harsin-Sahneh thrust sheets, in the Kermanshah radiolarite–ophiolite complex. These AFT ages closely match the radiometric ages of the ophiolites (85 Ma, Delaloye & Desmons, 1980), and may thus be related to oceanic crust generation (Fig. 13).

The 66 ± 30 Ma grain-age population, recorded by sample SH164 (Agha Jari Formation in the Zarrinabad syncline) (Fig. 10), may represent either a partially reset late Cretaceous age or a distinct cooling episode that took place during Maastrichtian times. This period of time was characterized by stacking and thrusting of the Kermanshah Complex and subsequent deformation of the margin of the Arabian plate from Santonian–Campanian to late Paleocene–early Eocene times (Berthier *et al.*, 1974; Gidon *et al.*, 1974; Braud, 1987; Agard *et al.*, 2005). As a consequence of this tectonic emplacement, the Arabian plate flexed down to form the early foreland basin of the NW Zagros that was filled with the shallowing-upwards Amiran–Kashkan sedimentary succession (Alavi, 2004; Homke *et al.*, 2009) (Fig. 13). The thrust sheets corresponding to the Kermanshah Complex produced an uplifted region along the margin of the NW segment of the Arabian plate that was the source area for the foreland basin to the SW and for the Gaveh Rud domain to the NE (e.g. Barrier & Vrielynck, 2008).

Middle–late Eocene cooling

An important cooling episode, recorded by both detrital samples from the Agha Jari Formation and from the boulders of the Bakhtyari Formation in Kuh-e Farangui occurred in middle and late Eocene times, with AFT ages ranging from 45 to 35 Ma. Identified detrital grain-age populations are consistent with ages obtained from bedrock samples (Fig. 13). This cooling episode must be interpreted as representative of cooling/denudation episodes occurring in the source areas, mostly in the Sanandaj-Sirjan Zone around middle and late Eocene times, coevally with the main arc-related magmatism activity in SW Iran.

In the inner and central parts of the Zagros foreland basin in Lurestan Province, the middle and late Eocene were characterized by either a low rate of sediment accumulation or a sedimentary hiatus. Only ~320 m of Kahskan red beds accumulated and were preserved in the central part of the basin during a period that can be as long as 15 Myr, before the deposition of the shallow marine platforms of the Shahbazan Formation in early Oligocene time (Homke *et al.*, 2009). This low sediment supply (or nondeposition) in the Zagros foreland basin during the Paleocene–Eocene could be caused by pro-

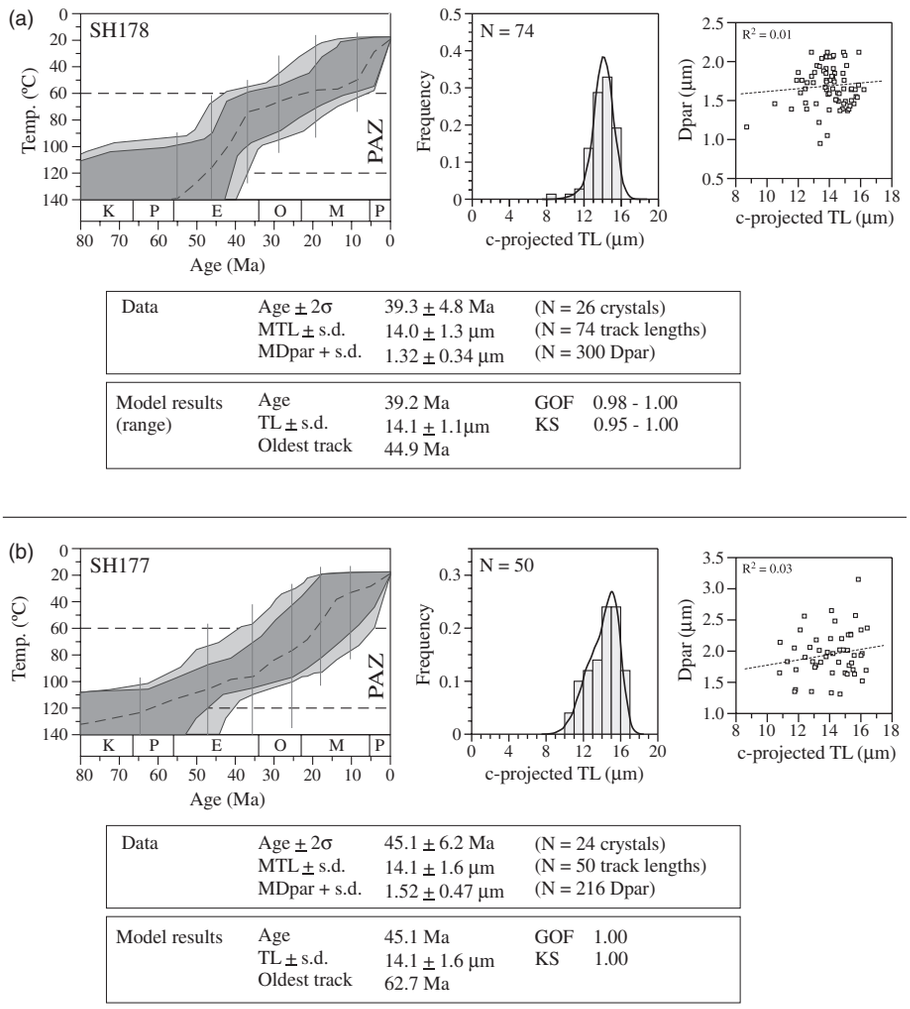

Fig. 12. Thermal-history modelling of metamorphic samples SH177 and SH178 (Kuh-e Farangui conglomerates, Fig. 6), carried out with AFTSolve® version 1.4.1 (Ketcham *et al.*, 2000). Good (dark grey) and acceptable (light grey) *T–t* envelopes were obtained for each sample by combining results of three models performed with distinct distributions of *T–t* constraints and using the Monte Carlo method with 50 000 steps. Best *T–t* paths (dashed lines) have been obtained using the Constrained Random Search method with 50 000 iterations (Ketcham *et al.*, 2000). *T–t* constraints used with Constrained Random Search modelling are represented by vertical grey lines. Central plots represent the comparison between the measured (histogram) and modelled (curves) track-length distributions; Dpar vs. track-length plots (maximum Dpar of the apatite grain on which the track length has been measured) are shown at right. The relatively low value of the linear regression parameter R^2 indicates absence of a clear relationship between Dpar and track length, particularly for sample SH178. GOF, goodness-of-fit probability; KS, Kolmogorov–Smirnov probability; PAZ, Partial Annealing Zone (Gleadow & Fitzgerald, 1987; Brown *et al.*, 1994).

gressive reduction of the topographic relief that formed during the tectonic emplacement of the ophiolitic–radiolaritic slices on top of the distal Arabian margin in late Cretaceous times. The lack of basin subsidence as well as moderate tectonic shortening observed for the middle and late Eocene in the Zagros foreland basin may be attributed to a shift of tectonic activity towards the NE along the Gaveh Rud domain and the front of the Sanandaj-Sirjan block, which were still separated from the Zagros foreland basin (e.g. Barrier & Vrielynck, 2008).

In effect, during the middle Eocene, intense flysch sedimentation filled up the deep Gaveh Rud sedimentary trough, between the Sanandaj-Sirjan Zone and the already deformed Arabian margin (Braud, 1987; Agard *et al.*, 2005). These Gaveh Rud sediments were mostly sourced from the Sanandaj-Sirjan Zone, with smaller contributions from the SW (the Kermanshah Complex on top of the Imbricated Zone). This deep marine trough trapped all the sediments supplied from the emerging Sanandaj-Sirjan Zone. The whole Gaveh Rud domain was then strongly folded in the late–middle Eocene, possibly announcing the collision between the Sanandaj-Sirjan block and Arabia (Braud, 1987; Agard *et al.*, 2005). Both the Gaveh Rud sedimentary domain and the Sanandaj-Sirjan Zone were subsequently intruded by numerous gabbroic plutons dated at 40–34 Ma (Leterrier, 1985; Braud, 1987) (Fig. 13). This short but intense plutonic activity shortly followed the cessation of calc-alkaline magmatism in the Sanandaj-Sirjan Zone and was partly coeval with intense Eocene calc-alkaline plutonic activity towards the NE, along the

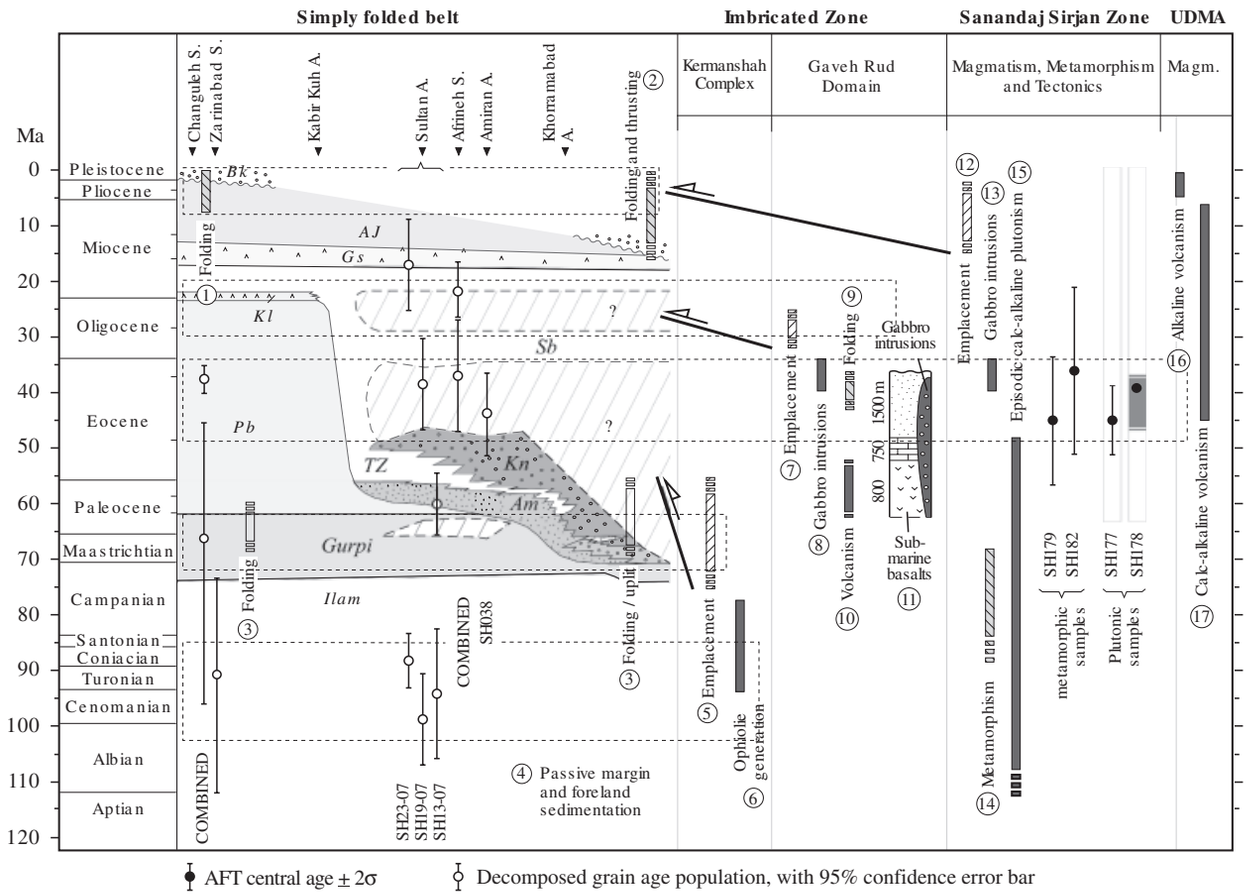

Fig. 13. Time chart, organized by structural zones, representing a compilation of sedimentary, tectonic and magmatic evidence for the geodynamic evolution of the NW Zagros orogen, and of apatite fission-track (AFT) results obtained in this study: detrital grain-age populations (COMBINED = ages obtained from the decomposition of combined grain-age populations measured on several samples, see Table 3), metamorphic/plutonic AFT ages, and thermal-history modelling results (with rapid cooling phases through the PAZ represented in grey). 'Emplacement' tectonic events mean emplacement of thrust slices on the Imbricated Zone. Kerman Complex, Kermanshah radiolarite–ophiolite Complex; Bk, Bakthyari Fm.; AJ, Agha Jari Fm.; Gs, Gachsaran Fm.; AS, Asmari Fm.; Kl, Kalhur Mb.; SB, Shahbazan Fm.; Pb, Pabdeh Fm.; Gu, Gurpi Fm.; Ks, Kashkan Fm.; Am, Amiran Fm.; UDMA, Urumieh Doktar Magmatic Arc. Compiled data are from (1) Homke *et al.* (2004). (2) Fakhari *et al.* (2008), Emami (2008). (3) Hessami *et al.* (2001), Fakhari & Soleimany (2003), Sherkati & Letouzey (2004), Fakhari *et al.* (2008), Homke *et al.* (2008). (4) James & Wynd (1965), Gidon *et al.* (1974), Braud (1987), Homke *et al.* (2004), Agard *et al.* (2005), Homke *et al.* (2008). (5) Berthier *et al.* (1974), Gidon *et al.* (1974), Braud (1987). (6) Delaloye & Desmons (1980). (7) Braud (1987), Agard *et al.* (2005). (8) Leterrier (1985), Braud (1987). (9–11) Braud (1987). (12) Braud (1971, 1987), Gidon *et al.* (1974), Agard *et al.* (2005), Molinaro *et al.* (2005), Fakhari *et al.* (2008). (13) Leterrier (1985), Braud (1987). (14) Mohajjel & Fergusson (2000). (15) Valizadeh & Cantagrel (1975), Berberian & Berberian (1981), Berberian *et al.* (1982), Masoudi (1997), Masoudi *et al.* (2002), Horton *et al.* (2008). (16 and 17) Bernard *et al.* (1979), Martel-Jentin *et al.* (1979), Berberian & Berberian (1981), Berberian *et al.* (1982), Bina *et al.* (1986).

Urumieh-Doktar magmatic arc and central Iran (Valizadeh & Cantagrel, 1975; Berberian & Berberian, 1981; Masoudi, 1997; Baharifar *et al.*, 2004; Horton *et al.*, 2008) (Fig. 13). These magmatic events have been attributed to transpressive movements by Leterrier (1985) and Braud (1987). Agard *et al.* (2005) and Ghasemi & Talbot (2006), however, proposed that slab breakoff occurred in the Eocene after the cessation of subduction beneath the Sanandaj-Sirjan Zone, consistently with the model proposed by Kestin *et al.* (2008) in north-central Turkey on the basis of magmatic evidence. An important gold mineralization event in the Sanandaj-Sirjan Zone during the Eocene (between ~56 and 38 Ma) might result from regional thermal disturbance and fluid input that have been attributed to this proposed slab breakoff beneath the Sanandaj-Sirjan Zone by Moritz *et al.* (2006).

Although the Sanandaj-Sirjan Zone was still separated from the Zagros foreland basin during the Eocene (e.g. Barrier & Vrielynck, 2008), slab breakoff would have produced regional uplift probably affecting the entire Zagros foreland basin. The absence of significant subsidence between deposition of the Amiran and Shahbazan Formations might be partly due to such regional uplift, but no clear indications for major uplift and denudation in the basin at that time are available. Significant fluid circulation, responsible for the alteration and remagnetization of Amiran sediments (Homke *et al.*, 2009), and probably participating to the recorded partial resetting of AFT ages,

were detected in the Amiran anticline, but their origin is not constrained. Geodynamic processes related to the Zagros orogeny other than slab breakoff, e.g. partial lithosphere delamination (Maggi & Priestley, 2005), must also be considered as possible causes for Eocene magmatic and tectonic activity recorded by AFT cooling ages.

The presence of rare coeval Eocene gabbro dykes in the NE Kermanshah ophiolitic units, i.e. on the NE border of the Arabian plate (Leterrier, 1985) suggests that the Sanandaj-Sirjan Zone was relatively close to the Arabian margin at that time, so that the southern Neo-Tethys realm was about to close in the late Eocene. The Gaveh Rud volcano-sedimentary domain was effectively thrust on top of the radiolaritic and ophiolitic thrust sheets of the Kermanshah Complex shortly after late Eocene emplacement of the gabbro intrusions, initiating the collision between the Arabian plate and the Sanandaj-Sirjan block. Thrusting of the Gaveh Rud tectonic unit was sealed by late Oligocene to early Miocene conglomerates (Braud, 1987; Agard *et al.*, 2005). In the early Oligocene, after the protracted middle and late Eocene quiescent period, the Zagros foreland basin subsided again, allowing deposition of the transgressive shallow marine Shahbazan limestones. Although very little is known of the lithospheric structure during and after the Eocene period, the onset of marine sedimentation (i.e. deposition of the Shahbazan Formation) in the study area during the Oligocene indicates that the lithosphere subsided, either as a result of cooling, flexure or both. This subsidence occurred relatively soon after the possible slab breakoff and was probably related to the effects of continuous compression with concomitant lithospheric thickening. A similar process has recently been proposed for the northern part of the Tibetan Plateau (Jiménez-Munt *et al.*, 2008).

Late Oligocene–early Miocene cooling

The late Oligocene–early Miocene cooling event at around 22 Ma is only documented by AFT grain-age populations from the Agha Jari sediments sampled in the Afrineh growth syncline (Fig. 10), and needs therefore to be confirmed by further analyses. These ages, however, are concurrent with large-scale observations that have been interpreted to show the final stages of closure of the Neo-Tethys by the collision of the Sanandaj-Sirjan domain against Arabia (e.g. Agard *et al.*, 2005; Horton *et al.*, 2008). Additional observations are the onset of Neogene foreland basin flexure and the interruption of the marine connection between the Mediterranean Sea and the Indo-Pacific Ocean (e.g. Harzhauser *et al.*, 2007).

During late Oligocene and early Miocene times, flysch sediments were deposited in the NE region of the Imbricated Zone before they were overthrust by the Sanandaj-Sirjan domain (Fig. 13). As consequence of Sanandaj-Sirjan thrusting, the foreland basin flexed down and was filled with the thick Asmari, Gachsaran and Agha Jari successions (e.g. James & Wynd, 1965; Allen *et al.*, 2004; Sherkati & Letouzey, 2004; Ahmadhadi *et al.*, 2007; Mouthereau *et al*, 2007). In addition, a new wave of folding propagated across the Zagros Simply Folded Belt, shaping the present day anticlines. Folding propagated towards the foreland and reached the front of the Pusht-e Kuh Arc around 7.6 ± 0.5 Ma (Homke *et al.*, 2004; Emami, 2008).

In the early Miocene, a relatively small unconformity developed in the foreland basin between the Shahbazan and Asmari Formations, roughly coeval with a marked decrease in sediment accumulation rates in the Dezful Embayment that started around 22 Ma (Ehrenberg *et al.*, 2007) (Fig. 13). After the deposition of the shallow-marine Asmari Formation, the marine gateway along the Zagros foreland, which connected the Mediterranean Sea and the Indo-Pacific Ocean, definitely closed in middle Miocene times (Harzhauser *et al.*, 2007).

CONCLUSIONS

Thermochronologic analyses presented in this study confirm the suitability of this method in the Zagros, although the number of usable apatites was low in most of the collected samples. Because this apparent lack of apatites and zircons in the Zagros foreland deposits, both detrital and *in situ* bedrock samples need to be collected across the different tectonic domains to precisely define the multiple collisional events of the Zagros Belt since late Cretaceous times.

Five families of AFT ages and grain-age populations have been obtained from both detrital (Amiran, Agha Jari and Bakhtyari Formations) and *in situ* bedrock samples. Although some of these ages may record partial annealing, they provide insights in distinct cooling/denudation events that occurred in the inner zones of the NW Zagros. These are (1) pre-middle Jurassic ($\sim$171, $\sim$225 Ma); (2) early–late Cretaceous ($\sim$91 Ma); (3) Maastrichtian ($\sim$66 Ma); (4) middle–late Eocene ($\sim$38 Ma); and (5) late Oligocene–early Miocene ($\sim$22 Ma).

The oldest (pre-middle Jurassic and early–late Cretaceous) AFT ages must be sourced from slices scratched from the outer Arabian margin and from the obducted oceanic radiolaritic–ophiolitic complex, respectively. Late Cretaceous AFT ages may correspond to partially reset older cooling ages or to the stacking of thrust sheets on top of the Arabian margin, which rapidly subsided to create the Amiran basin that was filled with the shallowing-upwards Amiran–Kashkan succession. This late Cretaceous–Paleocene event anticipated the Zagros collision *sensu stricto*.

The most representative AFT ages from this study show a major cooling/denudation event encompassing middle and late Eocene times (45–35 Ma), which coincides with massive volcanic and magmatic episodes in the Sanandaj-Sirjan tectonic domain that have been attributed by several authors to potential Neo-Tethys slab break-off beneath the Sanandaj-Sirjan block. Interestingly, this inferred major geodynamic event would have left little impact in the Zagros foreland, in which a protracted period of very slow or nondeposition occurred. This quiescent period for deposition and tectonics in the Zagros foreland basin was

the consequence of the migration of compression towards the NE, along the front of the Sanandaj-Sirjan domain and its associated Gaveh Rud fore-arc basin.

The last determined cooling phase, in the late Oligocene–early Miocene (~22 Ma), roughly corresponds to the onset of the second major phase of flexure after a protracted period of depositional and tectonic quiescence in the NE part of the Zagros foreland basin. This new period of flexure was characterized by the deposition of the thick Gachsaran and Agha Jari Formations. An early Miocene denudation event is in agreement with the final emergence of the area between Iran and Arabia as indicated by the closure of marine gateways along the Zagros foreland basin. During the Miocene and Pliocene, deformation propagated towards the foreland, completing the folding of the Zagros Fold Belt as well as the tightening of the different tectonic domains that existed between the Arabian and Iranian stable continental blocks.

The most recent tectonic pulses that led to the present Zagros Belt, despite their significance in the Zagros orogeny, are only recorded by the final (< 10 Myr) cooling and exhumation phases inferred from thermal modelling of detrital apatites collected in the Amiran deposits. For this reason, lower closure-temperature thermochronology methods (e.g. apatite (U-Th)/He with closure temperature of ~75 °C) must be used to recover the most recent cooling/exhumation record in the Zagros Belt. More extended thermochronology studies are moreover required to better investigate the significant Eocene tectonic and magmatic episode.

ACKNOWLEDGEMENTS

This study is a contribution of the Group of Dynamics of the Lithosphere (GDL) within the frame of a collaborative project with the StatoilHydro Oil and Energy Research Centre in Bergen (Norway). We thank the support in the field of Hydro Zagros Oil and Gas Tehran and the National Iranian Oil Company (NIOC). We also thank Ridvan Karpuz for fruitful discussion in the field. The University of Grenoble supported FT analyses. Josep Serra-Kiel from Universitat de Barcelona was responsible for large foraminifera dating. Gilen Bernaola from Universidad del País Vasco was responsible for nannoplankton dating. Carmen Galindo from Universidad Complutense de Madrid was responsible for strontium isotopic dating. This study was also partially supported by Team Consolider-Ingenio 2010 nr. CSD2006-00041 funded by the Spanish Government. We finally thank Associate Editor Brian Horton, two anonymous reviewers and Hugh Sinclair for their constructive reviews that helped to improve the manuscript.

REFERENCES

Agard, P., Omrani, J., Jolivet, J. & Mouthereau, F. (2005) Convergence history across Zagros (Iran): constraints from Collisional and earlier deformation. *Int. J. Earth Sci. (Geol. Rund.)*, **94**, 401–419.

Ahmadhadi, F., Lacombe, O. & Daniel, J.M. (2007) Early reactivation of basement faults in Central Zagros (Sw Iran): evidence from pre-folding fracture patterns in Asmari formation and lower tertiary paleogeography. In: *Thrust Belts and Foreland Basins from Fold Kinematics to Hydrocarbon Systems (Chapter 11)* (Ed. by O. Lacombe, J. Lavé, F. Roure & J. Vergés), *Front. Earth Sci.*, pp. 205–228. Springer, Berlin.

Alavi, M. (1994) Tectonics of the Zagros Orogenic Belt of Iran: new data and interpretations. *Tectonophysics*, **229**, 211–238.

Alavi, M. (2004) Regional stratigraphy of the Zagros fold-thrust belt of Iran and its Proforeland evolution. *Am. J. Sci.*, **304**, 1–20.

Allen, M., Jackson, J. & Walker, R. (2004) Late cenozoic reorganization of the Arabia-Eurasia collision and the comparison of short-term and long-term deformation rates. *Tectonics*, **23**, TC2008, doi:2010.1029/2003TC001530.

Babaei, A., Babaie, H.A. & Arvin, M. (2005) Tectonic evolution of the Neyriz Ophiolite, Iran: an accretionary prism model. *Ofioliti*, **30**, 65–74.

Baharifar, A., Moinevaziri, H., Bellon, H. & Pique, A. (2004) The crystalline complexes of Hamadan (Sanandaj-Sirjan Zone, Western Iran): metasedimentary mesozoic sequences affected by Late Cretaceous Tectono-Metamorphic and plutonic events. *Comp. Rend. Geosci.*, **336**, 1446–1452.

Barbarand, J., Carter, A., Wood, I. & Hurford, T. (2003a) Compositional and structural control of fission-track annealing in Apatite. *Chem. Geol.*, **198**, 107–137.

Barbarand, J., Hurford, T. & Carter, A. (2003b) Variation in Apatite fission-track length measurement: implications for thermal history modelling. *Chem. Geol.*, **198**, 77–106.

Barrier, E. & Vrielynck, B. (2008) Palaeotectonic maps of the Middle East: Middle East Basins Evolution Programme. Commission for the Geological Map of the World, CCGM-CGMW © 2008, 14pp.

Berberian, F. & Berberian, M. (1981) Tectono-plutonic episodes in Iran. In: *Zagros-Hindu Kush-Himalaya-Geodynamic Evolution* (Ed. by H.K. Gupta & F.M. Delany), *Geodynam. Ser.*, 3, pp. 5–32. American Geophysical Union, GSA and Ed. Board, Washington, DC.

Berberian, F., Muir, I.D., Pankhurst, R.J. & Berberian, M. (1982) Late cretaceous and early Miocene Andean-type plutonic activity in Northern Makran and Central Iran. *J. Geol. Soc. Lond.*, **139**, 605–614.

Berberian, M. (1995) Master "Blind" thrust faults hidden under the Zagros Folds: active basement tectonics and surface morphotectonics. *Tectonophysics*, **241**, 193–224.

Berberian, M. & King, G.C.P. (1981) Towards a paleogeography and tectonic evolution of Iran. *Can. J. Earth Sci.*, **18**, 210–265.

Bernard, D., Caillat, C., Dehlavi, P., Martel-Jentin, B. & Vivier, G. (1979) Premières Données Géochronométriques Sur Les Roches Intrusives De La Région De Saveh, Iran, 7ème R.A.S.T., Société Géologique de France, Lyon, 314pp.

Berthier, F., Billiault, J.-P., Halbronn, B. & Maurizot, P. (1974) Etude Stratigraphique Pétrologique Et Structural De La Région De Khorramabad. Unpublished PhD Thesis, Université de Grenoble, 281pp.

Bina, M.M., Bucur, I., Prevot, M., Meyerfeld, Y., Daly, L., Cantagrel, J.M. & Mergoil, J. (1986) Palaeomagnetism, petrology and geochronology of tertiary magmatic and sedimentary units from Iran. *Tectonophysics*, **121**, 303–329.

Blanc, E., Vergés, J., Gillespie, P., Casciello, E., Emami, H., Homke, S., Ghoodarzi, M.H.G., Egebjerg, T., Valinejad, M., Hunt, D., Sharp, L., Livbjerg, F., Efstathiou, J.,

Skott, P., Taati, F. & Rasmussen, E. (2008) Field evidences for a major Early Paleogene folding phase in the Zagros Simple folded Zone. Conference Proceedings "Fold and thrust belt exploration" Petroleum Group Tectonic Studies Group, Geological Society of London, 14–16 May 2008, Abstracts Book, 24pp.

Brandon, M.T. (1992) Decomposition of fission-track grain-age distributions. *Am. J. Sci.*, **292**, 535–564.

Braud, J. (1970) Les Formations Du Zagros Dans La Région De Kermanshah (Iran) Et Leur Rapport Structuraux. *C. R, Acad. Sci. Paris*, **271**, 1241–1244.

Braud, J. (1987) La Suture Du Zagros Au Niveau De Kermanshah (Kurdistan Iranien): Reconstitution Paléogéographique, Évolution Géodynamique, Magmatique Et Structurale. Unpublished PhD Thesis, Universtié Paris-Sud, 488pp.

Brown, R.W., Summerfield, M.A. & Gleadow, A.J.F. (1994) Apatite fission track analysis: its potential for the estimation of denudation rates and implications for models of long-term landscape development. In: *Process Models and Theoretical Geomorphology* (Ed. by M.J. Kirkby), pp. 23–53. Wiley, Chichester.

Carlson, W.D., Donelick, R.A. & Ketcham, R.A. (1999) Variability of Apatite Fission-Track annealing kinetics: I. Experimental results. *Am. Mineral.*, **84**, 1213–1223.

Colman-Sadd, S.P. (1978) Fold development in Zagros simply folded belt, Southwest Iran. *Am. Assoc. Petrol. Geol. Bull.*, **62**, 984–1003.

Delaloye, M. & Desmons, J. (1980) Ophiolites and Melange Terranes in Iran: a geochronological study and its paleotectonic implications. *Tectonophysics*, **68**, 83–111.

Donelick, R.A. (1991) Crystallographic orientation dependence of mean etchable fission track length in apatite; an empirical model and experimental observations. *American Mineralogist*, **76**, 83–91.

Donelick, R.A., Ketcham, R.A. & Carlson, W.D. (1999) Variability of apatite fission-track annealing kinetics: II. Crystallographic orientation effects. *Am. Mineral.*, **84**, 1224–1234.

Dumitru, T.A. (1993) A new computer-automated microscope stage system for fission-track analysis. *Nucl.Tracks Radiat.Meas.*, **21**, 575–580.

Ehrenberg, S.N., Pickard, N.A.H., Laursen, G.V., Monibi, S., Mossadegh, Z.K., Svånå, T.A., Aqrawi, A.A.M., McArthur, J.M. & Thirlwall, M.F. (2007) Strontium isotope stratigraphy of the asmari formation (Oligocene–Lower Miocene), SW Iran. *J Petrol. Geol.*, **30**(2), 107–128.

Emami, H. (2008) Foreland propagation folding and structure of the Mountain Front Flexure in the Pusht-e Kuh Arc (NW Zagros, Iran). Unpublished PhD Thesis, Universitat de Barcelona, pp. 1–180.

Emami, H., Vergés, J., Nalpas, T., Gillespie, P., Sharp, I., Karpuz, R., Blanc, E.P. & Goodarzi, M.G.H. (in press). Structure of the mountain front flexure along the Anaran anticline in the Pusht-e Kuh Arc (NW Zagros, Iran): insights from sand box models. In: *Tectonic and Stratigraphic evolution of Zagros and Makran during the Meso-Cenozoic*, (Ed. by P. Leturmy & C. Robin), *Geol. Soc. Lond. Spec. Vol.*, London.

Fakhari, M. & Soleimany, B. (2003) Early Anticlines of the Zagros Fold Belt, south west Iran. 2003 GSA Seattle Annual Meeting, 2–5 November 2003, Paper No. 156–23.

Fakhari, M.D., Axen, G.J., Horton, B.K., Hassanzadeh, J. & Amini, A. (2008) Revised age of proximal deposits in the Zagros Foreland Basin and implications for cenozoic evolution of the High Zagros. *Tectonophysics*, **451**, 170–185.

Falcon, N.L. (1961) Major earth-flexuring in the Zagros Mountains of South-West Iran. *Q. J. Geol. Soc. Lond.*, **117**, 367–376.

Falcon, N.L. (1974) Southern Iran: Zagros Mountains. In: *Mesozoic-Cenozoic Orogenic Belts. Data for Orogenic Studies*, **4** (Ed. by A.M. Spencer), *Geol. Soc. India, Spec. Publ.*, pp. 199–211. Edinburgh.

Galbraith, R.F. & Green, P.F. (1990) Estimating the component ages in a finite mixture. *Int. J. Radiat. Appl. Instrum. Part D. Nucl. Tracks Radiat. Meas.*, **17**, 197–206.

Galbraith, R.F. & Laslett, G.M. (1993) Statistical models for mixed fission-track ages. *Nucl. Tracks Radiat. Meas.*, **21**, 459–470.

Ghasemi, A. & Talbot, C.J. (2006) A new tectonic scenario for the Sanandaj-Sirjan Zone (Iran). *J. Asian Earth Sci.*, **26**, 683–693.

Ghazi, A.M. & Hassanipak, A.A. (1999) Geochemistry of Sub-alkaline and Alkaline Extrusives from the Kermanshah Ophiolite, Zagros Suture Zone, Western Iran: implications for Tethyan plate tectonics. *J. Asian Earth Sci.*, **17**, 319–332.

Gidon, M., Berthier, F., Billiautt, J.-P., Halbronn, B. & Maurizot, P. (1974) Sur Quelques Caractères De La Tectonique Néocrétacée Dans La Région De Borudjerd (Zagros Oriental, Iran). *C. R. Acad. Sci. Paris*, **278**, 577–580.

Gleadow, A.J.W. (1981) Fission-track dating methods: what are the real alternatives? *Nucl. Tracks*, **5**, 3–14.

Gleadow, A.J.W. & Fitzgerald, P.G. (1987) Uplift history and structure of the Trans-Antarctic Mountains: new evidence from fission track dating of basement apatites in the Dry Valleys Area, Southern Victoria Land. *Earth Planet. Sci. Lett.*, **82**, 1–14.

Glennie, K. (1995) *The Geology of the Oman Mountains. An Outline of Their Origin*, 1st edn. Scientific Press Ltd, Beaconsfield, UK.

Golonka, J. (2004) Plate tectonic evolution of the Southern Margin of Eurasia in the Mesozoic and Cenozoic. *Tectonophysics*, **381**, 235–273.

Gong, Z., Dekkers, M.J., Dinarès-Turell, J. & Mullender, T.A. (2008) Remagnetization mechanism of lower cretaceous rocks from the Organya basin (Pyrenees, Spain). *Stud. Geophys. Geod.*, **52**, 187–210.

Harzhauser, M., Kroh, A., Mandic, O., Piller, W.E., Göhlich, U., Reuter, M. & Berning, B. (2007) Biogeographic responses to geodynamics: a key study all around the Oligo–Miocene Tethyan Seaway. **246**, 241–256.

Hempton, M.R. (1985) Structure and deformation history of the Bitlis Suture near Lake Hazar, Southeastern Turkey. *Geol. Soc. Am. Bull.*, **96**, 233–243.

Hempton, M.R. (1987) Constraints on Arabian plate motion and extensional history of the Red-Sea. *Tectonics*, **6**, 687–705.

Hessami, K., Koyi, H.A., Talbot, C.J., Tabasi, H. & Shabanian, E. (2001) Progressive unconformities within an evolving foreland fold-and-thrust belt, Zagros Mountains. *Geol. Soc., Lond.*, **158**, 969–981.

Homke, S., Vergés, J., Garcés, M., Emami, H. & Karpuz, R. (2004) Magnetostratigraphy of Miocene–Pliocene Zagros foreland deposits in the front of the Push-E Kush Arc (Lurestan Province, Iran). *Earth Planet. Sci. Lett.*, **225**, 397–410.

Homke, S., Vergés, J., Serra-Kiel, J., Bernaola, G., Sharp, I., Garcés, M., Montero-Verdú, I., Karpuz, R. & Goodarzi, M.H. (2009) Late Cretaceous–Paleocene formation of the proto–Zagros foreland basin, Lurestan Province, SW Iran. *Geol. Soc. Am. Bull.*, **121**, 963–978, doi: 910.1130/B26035.26031.

Hooper, R.J., Baron, I.R., Agah, S. & Hatcher, R.D. Jr. (1994) The cenomanian to recent development of the Southern

Tethyan Margin in Iran. In: *Middle East Petroleum Geosciences Geo*, **II** (Ed. by M.I. Al-Husseini), *Gulf Petro Link, Barhein*, pp. 505–516.

Horton, B.K., Hassanzadeh, J., Stockli, D.F., Axen, G.J., Gillis, R.J., Guest, B., Amini, A., Fakhari, M.D., Zamanzadeh, S.M. & Grove, M. (2008) Detrital zircon provenance of neoproterozoic to cenozoic deposits in Iran: implications for Chronostratigraphy and Collisional tectonics. *Tectonophysics*, **451**, 97–122.

Hurford, A.J. & Green, P.F. (1982) A users' guide to fission track dating calibration. *Earth Planet. Sci. Lett.*, **59**, 343–354.

Hurford, A.J. & Green, P.F. (1983) The zeta age calibration of fission-track dating. *Chem. Geol. (Isotope Geosci. Sec.)*, **1**, 285–317.

Hurford, A.J. & Hammerschmidt, K. (1985) 40Ar/39Ar dating of the Bischop and Fisch Canyon Tuffs: calibration ages for fission-track dating standards. *Chem. Geol.*, **58**, 23–32.

Jahangiri, A. (2007) Post-collisional Miocene adakitic volcanism in NW Iran: geochemical and geodynamic implications. *J. Asian Earth Sci.*, **30**, 433–447.

James, G.A. & Wynd, J.G. (1965) Stratigraphic Nomenclature of Iranian Oil Consortium Agreement Area. *Bull. Am. Assoc. Petrol. Geol.*, **49**, 2182–2245.

Jiménez-Munt, I., Fernàndez, M., Vergés, J. & Platt, J.P. (2008) Lithosphere structure underneath the Tibetan Plateau Inferred from Elevation, Gravity and Geoid Anomalies. *Earth Planet. Sci. Lett.*, **267**, 276–289.

Juez-Larré, J. & Andriessen, P.A.M. (2006) Tectonothermal evolution of the northeastern margin of Iberia since the break-up of Pangea to present, revealed by low-temperature fission-track and (U-Th)/He Thermochronology: a case history of the catalan coastal ranges. *Earth Planet. Sci. Lett.*, **243**, 159–180.

Kestin, M., Genç, Ş.C. & Tüysü, O. (2008) Petrology and geochemistry of post-collisional Middle Eocene volcanic units in North-Central Turkey: evidence for magma generation by slab breakoff following the closure of the Northern Neotethys Ocean. *Lithos*, **104**, 267–305.

Ketcham, R.A., Donelick, M.B. & Carlson, W.D. (1999) Variability of apatite fission-track kinetics: Iii. Extrapolation to geological time scales. *Am. Mineral.*, **84**, 1235–1255.

Ketcham, R.A., Donelick, R.A. & Donelick, M.B. (2000) Aftsolve: A program for multi-kinetic modeling of Apatite Fission-Track Data. *Geol. Mater. Res.*, **2**, 1–32.

Leterrier, J. (1985) Mineralogical, Geochemical and isotopic evolution of two Miocene mafic intrusions from the Zagros (Iran). *Lithos*, **18**, 311–329.

Maggi, A. & Priestly, K. (2005) Surface waveform tomography of the Turkish-Iranian Plateau. *Geophysical Journal International*, **160**, 1068–1080.

Martel-Jentin, B., Caillat, C., Dehlavi, P. & Vivier, G. (1979) Géochimie Du Volcanisme Et Du Plutonisme Paléogènes De La Région De Saveh (Iran). Origine Des Tendances Alcalines Et Calco-Alcalines Du Paléogène De La Zone De L'iran Central. 7ème R.A.S.T, Société Géologique de France, Lyon, 314pp.

Martini, E. (1971) Standard Tertiary and Quaternary calcareous nannoplankton zonation. In: Second Planktonic Conference, Rome, pp. 739–785.

Masoudi, F. (1997) Contact Metamorphism and Pegmatite Development in the SW of Arak, Iran. PhD Thesis, The University of Leeds, UK, 231pp.

Masoudi, F., Yardle, B.W.D. & Cliff, R.A. 2002 Rb/Sr geochronology of pegmatites, plutonic rocks and hornfels in the region south west of Arak, Iran. *Iran. J. Sci.*, **13**, 249–254.

McArthur, J.M. & Howarth, R.J. (2004) Strontium isotope stratigraphy. In: *A Geologic Time Scale 2004: Cambridge* (Ed. by A.G. Smith), pp. 96–105. Cambridge University Press, Cambridge.

McCall, G.J.H. (1999) The geotectonic history of the Makran and Adjacent Areas of Southern Iran. *J. Asian Earth Sci.*, **15**, 517–531.

McQuarrie, N., Stock, J.M., Verdel, C. & Wernicke, B.P. (2003) Cenozoic evolution of Neotethys and implications for the causes of plate motions. *Geophys. Res. Lett.*, **30**, 2036, doi:2010.1029/2003GL017992, 012003.

Mohajjel, M. & Fergusson, C.L. (2000) Dextral transpression in Late Cretaceous Continental Collision, Sanandaj-Sirjan Zone, Western Iran. *J. Struct. Geol.*, **22**, 1125–1139.

Molinaro, M., Leturny, P., Guezou, J.-C., Frizon De Lamotte, D. & Eshraghi, S.A. (2005) The structure and kinematics of the south-eastern Zagros fold thrust belt; Iran: from thin-skinned to thick-skinned tectonics. *Tectonics*, **24**, TC3007, doi:10.1029/2004TC001633.

Moritz, R., Ghazban, F. & Singer, B. (2006) Eocene gold ore formation at Muteh, Sanandaj-Sirjan Tectonic Zone, Western Iran: a result of late-stage extension and exhumation of metamorphic basement rocks within the Zagros Orogen. *Econ. Geol.*, **101**, 1497–1524.

Mouthereau, F., Tensi, J., Bellahsen, N., Lacombe, O., De Boisgrollier, T. & Kargar, S. (2007) Tertiary sequence of deformation in a thin-skinned/thick-skinned collision belt: the Zagros Folded Belt (Fars, Iran). *Tectonics*, **26**, TC5006, doi:5010.1029/2007TC002098.

Naeser, C.W. & Fleischer, R.L. (1975) Age of the apatite at Cerro de Mercado, Mexico: a problem for fission-track annealing corrections. *Geophys. Res. Lett.*, **2**, 67–70.

Perch-Nielsen, K. (1981) Les nannofossiles calcaires à la limite Crétacé-Tertiaire prés de El Kef, Tunisie. *Cahiers Micropal.*, **3**, 25–37.

Perch-Nielsen, K. (1985) Cenozoic calcareous nannofossils. In: *Plankton Stratigraphy: Cambridge* (Ed. by H.M. Bolli, J.B. Saunders & K. Perch-Nielsen), pp. 427–554. Cambridge University Press, Cambridge.

Pignatti, J., Matteucci, R., Parlow, T. & Fantozzi, L. (1998) Larger foraminiferal biostratigraphy of the Maastrichtian-Ypresian Wadi Mashib succession (South Hadramawt Arch, SE Yemen). *Zeits. Geol. Wiss.*, **26**, 609–635.

Ravaut, P., Bayer, R., Hassani, R., Rousset, D. & Al Yahya'ey, A. (1997) Structure and evolution of the Northern Oman Margin: gravity and seismic constraints over the Zagros–Makran–Oman Collision zone. *Tectonophysics*, **279**, 253–280.

Ravenhurst, C.E., Willett, S.D., Donelick, R.A. & Beaumont, C. 1994 Apatite fission track thermochronometry from central Alberta: implications for the thermal history of the Western Canada Sedimentary Basin. *J. Geophys. Res.*, **99**, 20023–20042.

Ricou, L.E., Braud, J. & Brunn, J.H. (1977) Le Zagros. *Mém. H. Sér. Soc. Géol. France*, **8**, 33–52.

Robertson, A.H.F. (2006) Contrasting modes of ophiolite emplacement in the Eastern Mediterranean Region. In: *European Lithosphere Dynamics, Memoirs*, **32** (Ed. by D.G. Gee & R.A. Stephenson), pp. 235–261. Geological Society, London.

Rögl, F. (1998) Palageographic considerations for Mediterranean and Paratethys Seaways (Oligocene to Miocene). *Ann. Naturhistor. Mus.Wien.*, **99**, 279–310.

Sella, G.F., Dixon, T.H. & Mao, A. (2002) REVEL: a model for Recent plate velocities from space geodesy. *J. Geophys. Res.*, **107**(B4), 2081, doi:10.1029/2000JB000033.

Sherkati, S. & Letouzey, J. (2004) Variation of structural style and basin evolution in the Central Zagros (Izeh Zone and Dezful Embayment), Iran. *Mar. Petrol. Geol.*, **21**, 535–554.

Smout, A.H. (1954) Lower Tertiary Foraminifera of the Qatar Peninsula Natural History, British Museum, London, 96pp.

Stewart, R.J. & Brandon, M.T. (2004) Detrital-Zircon Fission-Track Ages for The "Hoh Formation": implications for Late Cenozoic Evolution of the Cascadia Subduction Wedge. *Geol. Soc. Am. Bull.*, **116**, 60–75.

Stöcklin, J. (1968) Structural history and tectonics of Iran: a review. *Am. Assoc. Petrol. Geol. Bull.*, **52**, 55–60.

Stoneley, R. (1990) The Arabian continental margin in Iran during the Late Cretaceous. In: *The Geology and Tectonics of the Oman Region* (Ed. by A.H.F. Robertson, M.P. Searle & A.C. Ries), pp. 787–795. Geological Society, London.

Travé, A., Labaume, P. & Vergés, J. (2007) Fluid systems in Foreland Fold-and-thrust belts: an overview from the Southern Pyrenees. In: *Thrust Belts and Foreland Basins from Fold Kinematics to Hydrocarbon Systems (Chapter 5)* (Ed. by O. Lacombe, J. Lavé, F. Roure & J. Vergés, *Front. Earth Sci.*, pp. 93–116. Springer, Berlin.

Valizadeh, M.V. & Cantagrel, J.M. (1975) K-Ar and Rb-Sr Radiometric Data on Micas from Mt-Alvand Granitic Complex near Hamadan (Western Iran). *Comp. Rend. l'Acad. Sci.*, **281**, 1083–1086.

van der Beek, P., Robert, X., Mugnier, J.-L., Bernet, M., Huyghe, P. & Labrin, E. (2006) Late Miocene – recent exhumation of the central himalaya and recycling in the Foreland Basin assessed by Apatite Fission-Track Thermochronology of Siwalik Sediments, Nepal. *Basin Res.*, **18**, 413–434.

Vergés, J. (2007) Drainage responses to oblique and lateral thrust ramps: a review. In: *Sedimentary Processes, Environments and Basins: A Tribute to Peter Friend (Chapter 3)*, **Vol. 38** (Ed. by G. Nichols, C. Paola & E. Williams, Int. Assoc. Sediment., Spec. Publ., pp. 29–47. Blackwell Publishing, Oxford.

Vergés, J., Karpuz, R., Efstatiou, J., Goodarzi, M.H., Emami, H. & Gillespie, P. (in press). Multiple detachment folding in Pusht-E Kuh Arc, Zagros. Role of Mechanical Stratigraphy. In: *AAPG Memoir on "Thrust Fault Related Folding"* (Ed. by K. McClay, J. Shaw & J. Suppe). AAPG Memoir, Tulsa, OK.

Manuscript received 11 February 2009; Manuscript accepted 6 August 2009.

